2023

Laboratory Experimentation and Numerical Modeling to Enhance Drainage in Geotextile Tubes

Jonah G. Tyson
West Virginia University, jt0031@mix.wvu.edu

2023

Laboratory Experimentation and Numerical Modeling to Enhance Drainage in Geotextile Tubes

Jonah G. Tyson

Laboratory Experimentation and Numerical Modeling to Enhance Drainage in Geotextile Tubes

Jonah G. Tyson

Thesis submitted to the

Benjamin M. Statler College of Engineering and Mineral Resources

at West Virginia University

in partial fulfillment of the requirements for the degree of

Master of Science in

Civil and Environmental Engineering

John Quaranta, Ph.D., P.E., Chair

Leslie Hopkinson, Ph.D.

Jason Fillhart, M.S., M.ED.

Wadsworth Department of C.E.E.

Morgantown, West Virginia

2023

Keywords: Filtration, Hydraulic Conductivity, Geotextile, Finite Element Modeling, Moisture Distribution, Dewatering

ABSTRACT

Laboratory Experimentation and Numerical Modeling to Enhance Drainage in Geotextile Tubes

Jonah G. Tyson

Geotextile fabrics are commonly used in the dewatering and filtration of high-water content geomaterials. Acid Mine Drainage (AMD) sludge is a geomaterial and has increasing production volumes in West Virginia. The WVDEP has large sludge storage sites for dewatering and long-term disposal. Currently the AMD is treated then transferred by pumping the material into geobags for long-term disposal in tubular shape geotextile bags that dewater the sludge. The current design of the geobags limit the pathways for the water to filter out due to the quality of the material. This research investigates the geotextile fabrics currently used and explores options to insert internal lateral drains to shorten drainage paths and accelerate dewatering.

AMD sludge was collected from the field to determine the current geotextile filtration and dewatering efficiencies with and without polymer additives. Analysis of column filtration tests concluded that a nonwoven geotextile exhibited the highest filtration efficiency (>91%) and a relatively efficient drainage hydraulic conductivity ($1.5x10^{-3}$ cm/s) for all permutations tested. The influence of polymer dosing on the AMD sludge indicated that for the no-polymer dose condition and a woven geotextile, the sludge hydraulic conductivity stabilized at $3x10^{-4}$ cm/s after approximately 50 hrs but had a filtration efficiency of 75 % particle retention. In contrast, the 20 ppm cation polymer dosed sludge exhibited a hydraulic conductivity at $3x10^{-5}$ cm/s within 150 hrs and a filtration efficiency of 91%. The polymer dosed sludge is preferred for minimizing solids pass through for environmental permit compliance.

Field *in situ* moisture and total solids percentage testing was performed on several AMD sludge filled geobags. Results indicated that dewatering trends are not consistent between bags and there was no clear placement location or position for installing internal lateral drains to enhance drainage.

ACKNOWLEDGEMENTS

I would like to express my deepest appreciation to my advisor, Dr. John Quaranta, for giving me the opportunity to engage in this research project, and for his assistance, support, encouragement, and guidance as an outstanding teacher, advisor, and mentor.

I am also grateful to Dr. Leslie Hopkinson and Jason Filhart for serving on my research advisory committee and for being there for any questions I had during the duration of my research project.

I would like to extend my sincere thanks to Iuri Santos and Titus Smith for their assistance in laboratory testing, as well as the mentorship and guidance throughout my research and the beginning of my graduate degree studies.

Special thanks to Luke Daugherty for his assistance in all my laboratory testing and all the field visits that occurred in order to complete my research project.

I wish to also thank Cory Nasiadka and Brady Watters for their assistance in laboratory and field testing.

Finally, I must express my very profound gratitude to my parents for providing me with unfailing support and encouragement throughout my years of study and through the process of researching and writing this thesis. This accomplishment would not have been possible without them. Thank you.

Table of Contents

List of Figures

List of Tables

1.0 Research Purpose, Scope, and Objectives

1.1 Purpose

The purpose of this research is to evaluate geotextile materials, installation location, and dewatering mechanisms for use as lateral drainage composites to dewater high moisture content sludge using geotextile tubes. The sludge that we will be using is a hydroxide sludge that is a precipitated form of Acid Mine Drainage (AMD) treatment. The ability to dewater the AMD sludge increases the soil solids, reduces the sludge disposal, and simplifies the methods for reuse. The purpose of this research will be to develop a method that will enhance the dewatering of the geotextile tubes.

1.2 Objectives & Scope

The objective of this research is to develop a passive method that will enhance dewatering in the geotextile tubes by incorporating internal lateral drainage materials. This will be done by investigating the following items:

1. Perform column filtration testing of geotextile fabrics as lateral drainage elements and investigate filtration and dewatering efficiencies to maximize total solids content,
2. Perform field testing of AMD filled geobags to identify the total solids distribution and dewatering characteristics, and
3. Develop a predictive numerical finite-element model of the geobag to simulate and quantify the dewatering process.

This research is performed following American Society for Testing and Materials (ASTM) manuals. Table 1 lists the ASTMs that were used during the duration of this research.

Table 1: ASTM's Used During Research

ASTM's Used During Research	
ASTM #	**Title**
D2216 - 19	Standard Test Methods for Laboratory Determination of Water (Moisture) Content of Soil and Rock by Mass
D4491 - 22	Standard Test Methods for Water Permeability of Geotextiles by Permittivity
D4751 -21	Standard Test Methods for Determining Apparent Opening Size of a Geotextile
D5088 - 20	Standard Practice for Decontamination of Field Equipment Used at Waste Sites
D854 - 14	Standard Test Methods for Specific Gravity of Soil Solids by Water Pycnometer

1.2.1 Characterization of geotechnical properties of AMD Sludge

The flocculated sediments or sludge produced by Acid Mine Drainage Treatment is investigated to determine the geotechnical classifications and hydraulic permeability characteristics that affect filtration and drainage mechanisms and efficiency. Characterization of the filtration and dewatering behaviors are be evaluated using column filtration testing. The produced filter cake will be studied in order to quantify the hydraulic conductivity and filtration efficiencies in the presence of different geotextile fabrics (one woven, two non-woven, and 2 typar). From the testing results there will be two fabrics selected (one non-woven and one typar), that will be used in future designs and testing.

The material inside the geotextile tubes will be investigated to determine how the flow of moisture occurs in the field due to saturated and unsaturated flow. This testing will be performed by taking samples of sludge at different depths and from different points along the geotextile tubes width and length. Mapping out the total solids in the bag will be done by using a XYZ contour map where X is the distance from the center port, Y is the estimated height of sample collected, and Z is the total solids from that point. Where with these samples we will determine the moisture content in these locations in order to forecast the behavior in the field depending on the pumping cycle and how long the bags have been sitting since its last pump or initial rollout date. From the results a current model will be constructed in order to compare to future predictive models and other tubes currently in the field.

1.2.2 Numerical modeling

Results from the column testing were used to create numerical models that predict the moisture flow inside regular geotextile tubes and geotextile tubes with the internal lateral drain. The models will show the change in flow rate and the direction of flow as the moisture moves from the input port to the geotextile shell. The models without the lateral drain are compared to the models that were created by taking field data in order to see the differences and if they follow the same trend.

2.0 Literature Review

The purpose of the literature review is to identify previous work done by others to solve a similar problem. This will include information of Geotextile Tubes for dewatering and filtration of high-water content soils, characterization and treatment of Acid Mine Drainage, Prefabricated Vertical Drains and Capillary Fibers for dewatering, and existing techniques and methods of analysis in finite element modeling for dewatering using geotextiles.

2.1 Geotextile Tubes in Sludge Dewatering

Dewatering of high-water content geomaterials is an important progressive step for beneficial use, engineered applications, and successful remediation (Kutay & Aydilek, 2004). Examples of the most common high-water content geomaterials are industrial sludge, wastewater treatment sludge, mine tailings, bottom-sea dredged sediments, dioxin-contaminated sediments, agriculture waste, and fly ash slurries (Fowler et al., 2000; Kutay & Aydilek, 2004; Liao & Bhatia, 2005; Weggel & Dortch, 2012; Berilgen et al., 2016). These high-water content materials are classified as having a high compressibility and a very low shear strength. There are effective methods to dewater this material, but the most efficient and cost-effective method is by pumping the material into geotextile tubes. Owing to the reduction of dewatering time and surface area when compared to other dewatering methods (Kutay & Aydilek, 2004). The geotextile tubes are used to separate solids and water by using the geotextile as the filter and drainage media. Figure 1 shows a series of geotextile tubes that are currently dewatering a slurry of Acid Mine Drainage precipitate that was recently pumped into the tubes.

Figure 1: Geotextile tubes dewatering (Source: Tyson 2022)

Geotextile tubes are manufactured by sewing one or more layers of high strength permeable geotextile fabric together to form cylindrical containers. This system allows for adequate liquid flow with limited soil loss within the plan of the geotextile (Koerner, 1998, p.91). Typically, the geotextiles that are used to create the geotextile tubes are high-strength monofilament fibrillated woven geotextiles (Berilgen et al., 2016). The woven geotextile sheets used in the construction of the tubes generally have a relatively large pore size, which is termed as Apparent Opening Size (AOS) (Kutay & Aydilek, 2004). Geotextile tubes have other uses besides dewatering such as dike construction, shoreline protection structures, submerged as stability berms, groins, and sill structures for controlling erosion (Fowler et al., 2000; Liao & Bhatia, 2005). Using the geotextile tubes has advantages over other forms of dewatering because of its ability to dewater large volumes of slurries at high flowrates, its ability to transfer liquids, its higher efficiency, lower overall cost, less labor needed, and lower environmental impacts (Liao & Bhatia, 2005).

The thicker and more cohesive the slurry is the more difficult it is to dewater efficiently inside the geotextile tubes. Chemical conditioning is a way to improve the dewatering characteristics of the slurry which results in improving the efficiency of the geotextile tubes system. The chemical

introduced into the slurry is called a polymer, a carbon-based macromolecule, which was specifically designed for dewatering. Polymers are used in geotextile tube dewatering applications when they have a relatively high molecular weight emulsion. The way the polymer works is by pulling together the small solid particles and create larger flocs which then allows for water to separate and drain out of the tube. When no polymer is used in geotextile tube dewatering the results are shown to be unsatisfactory (Gaffney et al. 2011).

In order to dewater the geomaterials using the geotextile tubes the material is hydraulically pumped into the tubes. Material is initially pumped into the tubes and then after the bag is filled the material starts to dissipate or drain before the next stage of pumping occurs. The way that the material dissipates inside the tubes is by flowing through the pore openings of the geotextile tube. Where the solid particles are trapped due to their larger particle size and the water is able to flow out (Kutay & Aydilek, 2004). Normally the dewatering of sludge inside the geotextile tubes takes one to two months of repeating the fills and draining of material (Lawson, 2008). During each phase of dewatering the tube a filter cake accumulates along the geotextile's outer downgradient shell surface. This occurs because the solids are being aggregated against the geotextile's upgradient surface. The accumulation of the filter cake and the increased filter cake thickness establishes a constant hydraulic conductivity (k). This means it is a falling head test, whereas the gradient reduces the flow reduces and the filter's hydraulic conductivity remains constant. The rate of flow and gradient through the filter cake depends on the permittivity of the geotextile, the permeability of the filter cake, and the thickness of the filter cake (Weggel & Dortch, 2012). As the dewatering efficiency decreases the hydraulic conductivity also decreases. The AMD sludge contains a large amount of water bonded to the little solids. The content of bound water is one of the major influencing factors that limit sludge dewaterability (Wei et al., 2018).

2.2 Acid Mine Drainage

2.2.1 Acid Mine Drainage Formation and Characteristics

Acid Mine Drainage (AMD) is one of the most critical environmental problems that are a byproduct of mining (Kalin et al., 2006). Where AMD affects the water quality and poses a challenge for the water to be treated to quality needed for it be discharged from the mine. Following the Clean Water Act Section 402, where it requires the mine operations to treat the

AMD (Vass et al., 2019). AMD is a serious pollution problem to surface and groundwater due to its low pH and its high concentrations of heavy metals (Akril & Koldas 2005). In the Eastern United States about 90% of the AMD that is found in streams and rivers come from abandoned mines in the eastern United States. Surface mines and underground mines pose different problems in order to deal with the AMD.

Acid Mine Drainage is formed when pyrite-bearing mines oxidize after mining, highway constructs, and other large-scale excavations (Akril & Koldas, 2005; Skousen et al., 2000; Vass et al., 2019). The most common sulfides in coal regions are predominantly pyrite and marcasite (FeS_2), but other metals may be complexed with the sulfides forming chalcopyrite ($CuFeS_2$), covellite (CuS), galena (PbS), and sphalerite (ZnS). In general, AMD is formed in places where the material is sulfide-rich and carbonate-poor (Skousen et al., 2000). Kalin et al (2006) lists that the formation of AMD involves sulfide oxidation (1), ferrous iron oxidation (2), ferric iron hydrolysis (3), and the enhanced oxidation of ferric sulfide ions (4).

$$FeS_2 + {}^{7}/_{2}\, O_2 + H_2O \xrightarrow{yields} Fe^{2+} + 2SO_4^{2-} + 16H^+ \quad (1)$$

$$Fe^{2+} + {}^{1}/_{4}\, O_2 + H^+ \xrightarrow{yields} Fe^{3+} + {}^{1}/_{2}\, H_2O \quad (2)$$

$$Fe^{3+} + 3H_2O \xrightarrow{yields} Fe(OH)_3(s) + 3H^+ \quad (3)$$

$$FeS_2 + 14Fe^{3+} + 8H_2O \xrightarrow{yields} 15Fe^{2+} + 2SO_4^{2-} + 16H^+ \quad (4)$$

2.2.2 Acid Mine Drainage Treatment

AMD chemical treatment is accomplished by adding alkaline in order for the dissolved metal ions to precipitate as hydroxides and allow the clean water to be discharged into a stream where Calcium Carbonate ($CaCO_3$) acts as the neutralizing agent (Vass et al., 2019).

According to Skousen et al. (2000) there are six chemicals that are commonly used to treat the AMD. Each of these chemicals have different characteristics that would make it more suitable for different situations in order to treat the AMD. Some technical factors that can affect what chemical is chosen are:

- The acidity levels of the AMD
- The flow AMD
- Types of metals AMD
- Concentrations of metals in AMD

The economic factors are:

- Price of reagents
- Cost of labor
- Cost of machinery and equipment
- Number of years that the treatment will be needed
- The interest rate

The types of the chemicals that can be used are:

- Limestone (Calcium Carbonate - $CaCO_3$)
- Hydrated Lime (Calcium Hydroxide - $Ca(OH)_2$)
- Pebble Quicklime (Calcium Oxide - CaO)
- Soda Ash (Sodium Carbonate - Na_2CO_3)
- Caustic Soda (Sodium Hydroxide - $NaOH$)
- Ammonia (Anhydrous Ammonia - NH_3).

The most common chemical used to treat AMD is hydrated lime or Calcium Hydroxide. The hydrated lime is added to the AMD as a slurry mixture, where the dissolution of the hydrated lime (equation 5) causes the pH to increase and the metal ions to precipitate as hydroxides as shown for Fe in equation 6 (Kalin et al., 2006).

$$Ca(OH)_2 \xrightarrow{yields} Ca^{2+} + 2OH^- \quad (5)$$

$$Fe^{2+} + 2OH^- \xrightarrow{yields} Fe(OH)_2 \quad (6)$$

2.3 Drainage with Flocculated Slurry

Flocculation is the process of aggregating dispersed fine particles into larger flocs. This is done in three steps: destabilization, formation, and degradation. Destabilization eliminates any interparticle repulsion that opposes the aggregation of the particles. After destabilization, the floc forms and grows by collision and adhesion. The degradation of the floc is caused by the breakage of the aggregates due to shear and turbulence in the slurry (Hogg, 1999). The addition of a flocculant polymer would be introduced during the formation step, this will help promote floc growth.

Sludge dewatering is similar to the formation of a sludge cake in water. A sludge cake is formed by the aggregation of flocs in raw water. The properties of the floc affect the characteristics of the sludge cake and the dewatering performance (Wei et al., 2018). The size of the floc affects the dewatering performance where having a small floc size could factor into how well the sludge cake forms and a large floc size could cause for more water to bond with the solid material. Li et al. (2016), indicated that the compactness of the floc might play a larger role in sludge dewatering the floc size. The formation of the sludge cake also plays a role in dewatering of the sludge; this is because the compression of the sludge cake is another step-in sludge dewatering (Thapa et al., 2009). If the applied pressure exceeds a certain load, in the compression of the sludge cake, it will damage the sludge cake which could deteriorate the sludge filterability (Wei et al., 2018).

2.4 Prefabricated Vertical Drains for Dewatering Soft Saturated Clay

Prefabricated Vertical Drains (PVDs) are a type of geocomposite drain that are used to improve soil by shortening the drainage path to accelerate consolidation. PVDs were introduced to be an improvement to the sand drain since they are more efficient and cost effective. The most common PVDs are manufactured with a synthetic core that is enclosed by a geotextile fabric (Gabr et al., 1997). The geosynthetic drain consists of a corrugated polypropylene core with flow channels located on both sides and wrapped in a non-woven geotextile jacket (Warren et al., 2006). Each component of the PVD has a different function. The geotextile fabric is used as a

filter to inhibit the movement of soil particles from passing while allowing the water to drain. The fabric also prevents intrusion into the internal drain's flow paths under the lateral soil pressure. The functions of the synthetic core are to provide the internal drain flow paths, maintain the drain configuration and shape, and to provide support for the geotextile fabric as well as provide resistance due to longitudinal stretching and buckling of the drain (Rixner et al., 1986). PVDs are conventionally installed in a vertical direction but can be installed at any angle (Warren et al., 2006).

Indraratna et al. (2003) found that there are two factors that affect the PVD efficiency which are the smear zone and the well resistance. The smear zone is initially created during the installation of the PVD when using a mandrel. The extent of the smear zone is a function of the size and the shape of the mandrel. By installing the PVD with a mandrel there is a significant remolding of the subsoil that is in the immediate vicinity of the mandrel. The size of the smear zone has been estimated to be two to three times the equivalent diameter of the mandrel. The well resistance is caused by the resistance to the flow of water. The well resistance increases with the increase of the drains length which reduces the consolidation rate.

Gabr et al. (1997) states that PVDs follow the governing equation of consolidation which is expressed as:

$$\frac{\delta u}{\delta t} = c_r \left(\frac{\delta^2 u}{\delta r^2} + \frac{1}{r}\frac{\delta u}{\delta r}\right) + c_v \left(\frac{\delta^2 u}{\delta z^2}\right) \quad (7)$$

Where:

$c_r \; and \; c_v$ are the coefficients of consolidation in radial and vertical directions

u = excess pore pressure

r = radial distance from PVD

z = depth

In order to solve this equation, there are certain things that have to be assumed for the PVD's surrounding area. It is assumed that the outer boundary for the zone of influence is an impermeable membrane, meaning there is no flow through this zone, and that excess water is

only allowed to escape through the drain or the top of the zone. Another assumption is that the lower surface of the drain also acts a no flow boundary (Gabr et al 1997).

PVDs follow the conventional theory of consolidation which assumes that vertical drains are circular in cross section (Indraranta et al., 2003). PVDS are used as an application for the radial consolidation theory where the circumference of the PVD is more critical than the diameter (cross-sectional area) for accelerated consolidation (Gabr et al., 1997). Where the consolidation of the material is correlated with the change in the void ratio and with the increase of total solids in the sample. PVDs are typically used to consolidate soil (Warren et al., 2006).

PVDs typically are used to expedient consolidation of low permeability soils that are under a surface surcharge. They are also used to induce a hydraulic gradient which is done to promote the expulsion of water from the soil voids. PVDs are a more efficient and cost-effective method for improving soft soils with low hydraulic conductivities than other forms of drains (Gabr et al., 1997).

2.5 Dewatering by Capillary Fibers

Research by Azevedo and Zornberg (2013) found that under unsaturated conditions a capillary barrier can form that restricts water flow between two porous materials that have different hydraulic conductivities. This also can occur between a geotextile with a relatively large apparent opening size and a fine-grained soil. According to Zhang et al., (2014) a capillary barrier is a layer of coarse-grained soil or geosynthetic that reduces upward capillary flow of soil water due to the suction gradient generated by evaporation or freezing. The difference in the material's hydraulic conductivity will restrict the water from moving from the material with smaller pore spaces from entering into the material with the larger pores spaces, unless it reaches a certain suction level. Until that certain suction level is reached the moisture will build up in the fine-grained soils. In order to minimize the effect of the capillary barrier a special wicking fiber was used as an enhanced lateral drain. In order to show the effectiveness of the fabrics, Azevedo and Zornberg (2013) ran column tests to determine the formation of the capillary barrier, the effect of the lateral drainage, and the capillary barrier dissipation (Azevedo & Zornberg, 2013).

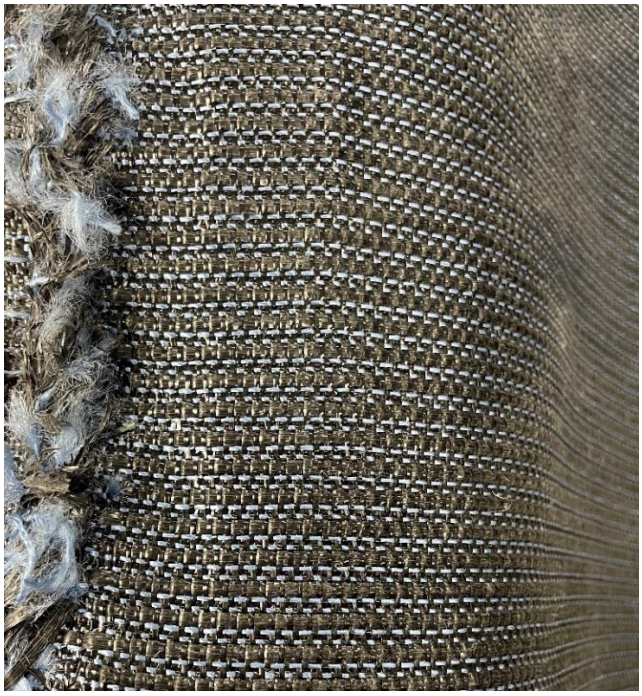

Figure 2: Capillary Fiber Example (Source: Tyson 2022)

Capillary fibers were used in the field to test moisture drainage in Alaskan roads (Zhang et al., 2014). The capillary wicking fabric was placed in the transverse direction of the road section so that the water would be transported in the direction towards the road's shoulder. Moisture distribution in the test area was shown in three different scenarios: with rainfall, during the freezing process, and during the thawing process. Data revealed that the soil closer to the wicking fabric had a lower moisture content than the soil the farthest away from the fabric's end, this data stayed consistent during the rainfall event. During the freezing and thawing processes, the wicking fabric showed little effect in changing the moisture content in the testing area. The slope of the wicking fabric can help drain the water under saturated conditions, but under unsaturated soils the wicking fabric relies on the suction gradient generated by the evaporation to drain the water.

2.6 Finite Element Modeling in Geotextile Drainage

In order to better understand the moisture distribution inside the geotextile tubes a 2-dimensional analysis using finite element modeling should be conducted. By using finite element model, we can create mathematical models that show present conditions and proposed conditions that could create a better dewatering (drainage) mechanism than the current design of the geotextile tubes that are currently in the field.

In Silva et al. (2021), their field study was to determine the changes in dimension of the geotextile tube during filling, and to record the final geotextile tube cross-section dimensions to use for the numerical modeling and analytical solution. Their goal was to better understand the mechanical behavior of the geotextile tube during the filling process. The numerical model developed was to simulate the process of filling a geotextile in the field; this was done by using the hydrostatic and internal pressure inside the bags to allow the model's height to reach the observed field height.

In Cantre' (2002) found that in order to create the model for the filling process it was necessary to apply fluid conditions to the filling material, however it was not possible to apply the same conditions for the consolidation and loading since the slurry drains from the geotextile bags. In their stacking model they were trying to receive information about the maximum tension and the deformation. They assumed before creating the model was that the tube had already been drained. Then in their drainage model it was to simulate the dewatering and the consolidation of the tubes. They found that as the water drains the pore pressure decreases and during the filling process is when the pore pressure is high and over saturated. Cantre' (2002) also found that the largest tension forces occurred during the filling process. So, when the geotextile bags were at their maximum capacity before the dewatering and consolidation began.

Numerical modeling can show different data when comparing the analytical results during the consolidation of the geotextile tubes (Brink et al., 2015). This is done by using one-dimension modeling to verify the results for both of these models before conducting a larger scale 2-dimensional model for drainage and compression. In the 2-dimensional analysis that model was initialized using a manual input of the initial pore pressure distribution. Assumptions for drainage only allowed for water to escape through the curved surface of the geotextile.

There are multiple ways to model what happens inside the geotextile tubes using 2-dimensional analysis and finite element modeling. Showing the filling process, dewatering and consolidation process, and the change in tension/deformation when creating a stack of geotextile tubes in the field. By making clear and concise assumptions about what occurs during each phase for the geotextile the numerical models should show the moisture distribution of the soil slurry. These are existing techniques used to drain high water content soil and soil like materials.

3.0 Laboratory Column Filtration Testing Approach

The purpose of this testing is to select the geosynthetic fabrics optimum wick drain fabric and to determine the optimum geotextile fabric by looking at their filtration efficiency, change in total solids, and their hydraulic conductivity by filtering and dewatering acid mine drainage (AMD) from two different WVDEP sites. Woven geotextiles, typically with larger AOS (apparent opening size), are conventional fabrics selected to dewater slurries in the form of geotextile tubes rather than using nonwoven fabrics. This is because woven geotextile fabrics have a significantly higher tensile strength, to withstand more radial stress from the high pressures of injection of the slurries into the tubes. These geotextile tubes are a common method for dewatering large volumes of slurries. This is done by pumping the slurries into the tubes and then allowing the slurry to passively dewatering inside the geotextile tube. Although the woven geotextile tubes are effective in filtration and dewatering over these slurries, they are not successful when the slurries have very fine particles that can pass through the gaps in the fabric. This study investigates the filtration and hydraulic conductivity of both woven and non-woven geotextile fabrics.

Once the filtration tests are completed. A wick drain fabric was selected to be used in the creation of a prototype geotextile tube dewatering system. There will also be a selected non-woven fabric that will also be used in prototype dewatering designs to help promote more filtration efficiency when combined with the woven geotextile fabric. The selected fabrics must efficiently capture the material from passing through the fabric but also allowing the water to flow through the filtration system.

3.1 Objective

The objective of the column filtration testing is to investigate the effectiveness and efficiency of each of the geotextile fabrics and how they dewater AMD slurry. This AMD slurry has either been treated by lime or has been completely dosed to the optimum dosage. From the testing a non-woven fabric will be selected to help with the filtration of AMD and a wick drain typar fabric will be selected to help promote more effective dewatering inside the geotextile tubes. Solids retention, system hydraulic conductivity (k), and change in solids content from the incoming slurry to the final output are being tested and analyzed to determine the dewatering and filtration efficiency for the fabrics/slurry system in order to produce the best fabrics to promote higher dewaterability.

3.2 Material Testing

A selection of geotextile fabrics was tested with a variation of AMD slurry treatment conditions. The treatment conditions included the preferred condition and the undesirable conditions to account for potential field conditions. The filtration and dewatering conditions evaluated include:

1. No Polymer Sludge from Omega Clarifier

2. 20 ppm Polymer T&T Sludge going to Geotextile Bags (20 ppm)

Five different geotextile fabrics were evaluated for the study. These fabrics that were tested had different uses in their field applications. The selection of the fabrics was based on fabric applications, AOS, and filtration efficiency. The geotextile specimens consisted of two typar fabrics used with the PVDs, one woven, and two nonwoven fabrics as present in Table 2.

Table 2: Geotextile Fabric Properties

Fabric Type		GT500 Woven	1100N Nonwoven	140NC Nonwoven	MD88 Nonwoven Typar	MD7407 Nonwoven Typar
Apparent Opening Size (mm)	ASTM D4751	0.425	0.15	0.212	0.09	0.23
Permittivity (sec^{-1})	ASTM D4491	N/A	0.8	2	0.3	0.4
Flow Rate ($L/min/m^2$)	ASTM D4491	815	3056	5704	N/A	N/A

3.3 Testing Procedure

The testing method used followed Weggel and Dortch (2012), who used column filtration test specimens consisting of a 5 cm clear PVC pipe mounted vertically to a wooden structure on a table. The PVC pipe has a ruler on the outside surface for measurements. The framing system secures the vertical tube to the table using a C-clamp. The selected geotextile is wrapped and tightened to the bottom of the pipe using a hose clamp. The fabric is mounted flush and covers the entire drainage surface area of the bottom of the pipe with no loose areas that could develop leakage. A graduated cylinder sits underneath the pipe to collect and measure the outflow. The outflow liquid is measured between time intervals to calculate the discharge flowrate.

3.3.1 Test Instructions

Preparation:

1.) Attach a clear tube with a ruler taped to the front and back to the stand using the white pipe strap. Only adjust the screws of the left side of the tube. Ensure the tube is level
2.) Cut about a 3-inch diameter piece of geotextile and tighten to the bottom of the tube using a hose clamp. Record dry mass of geotextile on the Tube Test data sheet
    a. Ensure the geotextile is pulled tight at the bottom of the tube so that it is flush. The geotextile should extend past the hose clamp in all directions.
    b. Be sure geotextile is facing the correct direction (heated side down)
3.) Place a 1000 mL graduated cylinder with a funnel underneath the bottom of the tube to collect the outflow
4.) Place a funnel on the top of the tub to pour the slurry in to the tube
5.) Obtain set volume of slurry (typically 500-1000 mL)
6.) Ensure that slurry is mixed thoroughly so that it is homogenous throughout while being careful to not break the floc structure
7.) Acquire three moisture content samples directly after slurry is mixed

Begin Test

1.) Once slurry is thoroughly mixed, start a stopwatch and immediately start to pour slurry into the tube

a. The funnel should be tilted while pouring the slurry to allow the slurry to run down the side of the tube to avoid the slurry splashing into the bottom of the tube as seen in Figure 3.

Figure 3: Tilted Funnel (Source: Nasiadka 2021)

b. Pour the slurry in at a rate of about 1 Liter per minute to ensure a slow pour as to not damage the floc structure of the slurry

2.) Once pouring is finished, record head, filter cake thickness and volume passed every 5 minutes where:

a. Head is the height of the water column in the tube
b. Volume passed is the volume that is collected in the bottom flask/graduate cylinder.
c. Filter cake thickness is the height of the filter cake (This may not be able to be read for the first couple minutes of the test)

Figure 4: Difference in head and thickness of filter cake (Source: Tyson 2022)

3.) After 20 minutes, readings can be taken at whatever interval is needed (at least once an hour)
4.) Once head is equal to filter cake thickness, pour DI or recirculate outflow (depending on the type of test). Record this in the data sheet
    a. Pour at the same rate of approximately 1 Liter per minute
    b. Use a small funnel and tilt to the side when pouring in an attempt to not damage the filter cake. The funnel should be rotated around the inside diameter of the tube to evenly distribute the pour around the circumference of the tube filter cake. This avoids an angled or uneven surface on top of the filter-cake
5.) Repeat step 4 for however many passes are necessary to develop a satisfactory system
6.) The test is complete when either:
    a. The filter cake thickness stops changing or
    b. Cracks start becoming visible within the filter cake
7.) Once complete, loose the hose clamp, carefully twist the and pull down to release the filter cake. Hold a bowl underneath the tube to catch the filter cake as it is pulled out of the tube. Liquid sample may come off.

8.) Record the moisture content of the filter cake from the top, bottom, and middle immediately after removing the filter cake.
9.) Scrape off all leftover filter cake from the geotextile and dry the geotextile in the oven. Weigh the dried geotextile to find the percent loss of solids.

Once the above parameters are dried and recorded the % Retained, % Lost, % Passing, Filtration Efficiency, and the hydraulic conductivity are calculated as shown by the equations below

$$\%\ Retained\ = \frac{solids\ retained\ (g)}{total\ solids\ (g)} x\ 100 \quad (8)$$

$$\%\ Lost\ = \frac{solids\ stuck\ in\ fabric\ (g)}{total\ solids\ (g)} x\ 100 \quad (9)$$

$$\%\ Passing\ = \frac{solids\ passing\ through\ fabric\ (g)}{total\ solids\ (g)} x\ 100 \quad (10)$$

$$Filtration\ Efficiency\ \%\ = \frac{total\ solids\ (g) - passing\ solids\ (g)}{total\ solids\ (g)} x\ 100 \quad (11)$$

$$Moisture\ Content\ (w\%) = \frac{water\ in\ filter\ cake\ (g)}{water\ in\ filter\ cake\ (g) + solids\ in\ filter\ cake\ (g)} x\ 100 \quad (12)$$

$$Hydraulic\ Conductivity\text{: } k\ = \frac{aL}{A\Delta t} ln(\frac{h1}{h2}) \quad (13)$$

Where:

a = cross-sectional area of the reservoir containing the influent liquid (cm^2)

L = length of the specimen (cm)

A = cross-sectional area of the specimen (cm^2)

Δt = elapsed time between determination of h1 and h2

h1 = head loss across the specimen, at time t1, m or cm

h2 = head loss across the specimen at time t2, m or cm

Hydraulic conductivity was calculated for each time step during testing. k values were averaged for each test once the steady state was reached per ASTM D5088-16a (ASTM 2016).

3.4 Results

The major results that are reported from the filter tests are the filtration efficiency, the total solid percentage of the slurry (inflow), the total solid percentage of the filter cake (output), and the hydraulic conductivity. The filtration efficiency is based on the weight of solids that do not pass through the filter compared to the weight solids that pass through the filter. The total solid from the output is the average between the top and the bottom after filtration is complete. The hydraulic conductivity is the average between each phase of the filtration test, where each test had 2 or 3 exposures. Where the first exposure was straight slurry and the second and third exposure being the addition of deionized water.

The first set of filter tests were run by using the No Polymer Sludge that was taken from the bottom of the clarifier at the Omega Site. This slurry was not dosed with polymer and only was treated with lime slurry. The fabrics tested in this set were the GT500, MD88 Typar, and MD7407 Typar. The GT500 fabric is the most common woven geotextile dewatering fabric, while the MD88 and MD7407 are both wicking drain Typar fabrics. The results for these tests are shown in Table 3-5.

Table 3: Initial No Polymer Omega GT500 Filtration Results

GT500 Data		Filtration	Slurry	Filter Cake	Hydraulic Conductivity		
Test #	Volume of DI Water Added (mL)	Filtration Eff.	Inflow TS	Output TS	k (cm/sec) initial	k (cm/sec) DI	k (cm/sec) DI (2nd)
1	500	91.61%	1.01 %	2.40%	$2.44x10^{-3}$	$1.71x10^{-4}$	-
4	1,000	93.80%	1.05 %	2.43%	$2.36x10^{-3}$	$1.46x10^{-3}$	$4.48x10^{-4}$
6	1,000	95.87%	1.40 %	2.28%	$1.25x10^{-3}$	$2.03x10^{-3}$	$1.22x10^{-3}$

Table 4: Initial No Polymer Omega MD88 Filtration Results

MD88 Data		Filtration	Slurry	Filter Cake	Hydraulic Conductivity		
Test #	Volume of DI Water Added (mL)	Filtration Eff.	Inflow TS	Output TS	k (cm/sec) initial	k (cm/sec) DI	k (cm/sec) DI (2nd)
3	1,000	94.83%	1.06%	2.07%	$2.09x10^{-3}$	$1.26x10^{-3}$	$6.43x10^{-4}$
5	1,000	96.21%	1.26%	2.40%	$3.46x10^{-3}$	$1.55x10^{-3}$	$5.06x10^{-4}$
8	1,000	95.79%	1.39%	2.69%	$1.59x10^{-3}$	$4.34x10^{-3}$	$2.88x10^{-3}$

Table 5: Initial No Polymer Omega MD7407 Filtration Results

MD7407 Data		Filtration	Slurry	Filter Cake	Hydraulic Conductivity		
Test #	Volume of DI Water Added (mL)	Filtration Eff.	Inflow TS	Output TS	k (cm/sec) initial	k (cm/sec) DI	k (cm/sec) DI (2nd)
2	500	92.72%	1.01%	2.31%	$1.97x10^{-3}$	$1.77x10^{-4}$	-
7	1,000	97.11%	1.40%	2.64%	$1.55x10^{-3}$	$3.45x10^{-3}$	$1.25x10^{-3}$
9	1,000	94.26%	1.41%	2.62%	$1.47x10^{-3}$	$2.46x10^{-3}$	$1.39x10^{-3}$

The second set of filter tests were also run using the No Polymer Sludge from the Omega Clarifier. The filters that were selected to be testing for this set were based on the filtration results from the first set. The fabrics that were tested in this set were the GT500, MD88, 140NC, and 1100N. Both the 140NC and 1100N are common woven fabrics which were selected to compare their relative efficiency. The results for the second set of tests are shown in Tables 6-9.

Table 6: Final No Polymer Omega GT500 Filtration Results

GT500 Data		Filtration	Slurry	Filter Cake	Hydraulic Conductivity		
Test #	Volume of DI Water Added (mL)	Filtration Eff.	Inflow TS	Output TS	k (cm/sec) initial	k (cm/sec) DI	k (cm/sec) DI (2nd)
10	1,000	63.03%	0.35%	1.66%	$1.47x10^{-3}$	$8.45x10^{-4}$	$9.74\ x10^{-4}$
13	1,000	48.79%	0.34%	2.09%	$4.20x10^{-3}$	$3.36x10^{-3}$	$2.50\ x10^{-3}$
15	1,000	77.80%	0.54%	1.54%	$3.14x10^{-3}$	$8.15x10^{-3}$	$5.46x10^{-3}$

Table 7: Final No Polymer Omega MD88 Filtration Results

MD88 Data		Filtration	Slurry	Filter Cake	Hydraulic Conductivity		
Test #	Volume of DI Water Added (mL)	Filtration Eff.	Inflow TS	Output TS	k (cm/sec) initial	k (cm/sec) DI	k (cm/sec) DI (2nd)
11	1,000	88.56%	0.70%	1.73%	$1.81x10^{-3}$	$2.38x10^{-3}$	$1.34x10^{-3}$
21	1,000	78.77%	0.46%	1.64%	$8.55x10^{-3}$	$1.43x10^{-3}$	$6.23x10^{-3}$
22	1,000	92.29%	0.49%	1.36%	$4.43x10^{-3}$	$4.80x10^{-3}$	$1.31x10^{-2}$

Table 8: Final No Polymer Omega 140NC Filtration Results

140NC Data		Filtration	Slurry	Filter Cake	Hydraulic Conductivity		
Test #	Volume of DI Water Added (mL)	Filtration Eff.	Inflow TS	Output TS	k (cm/sec) initial	k (cm/sec) DI	k (cm/sec) DI (2nd)
17	1,000	92.44%	0.48%	1.76%	$3.90x10^{-3}$	$2.35x10^{-3}$	$3.51x10^{-4}$
19	1,000	91.24%	0.46%	1.78%	$4.51x10^{-3}$	$2.12x10^{-3}$	$5.63x10^{-3}$
20	1,000	91.27%	0.46%	1.66%	$4.39x10^{-3}$	$9.50x10^{-4}$	$1.78x10^{-3}$

Table 9: Final No Polymer Omega 1100N Filtration Results

1100N Data		Filtration	Slurry	Filter Cake	Hydraulic Conductivity		
Test #	Volume of DI Water Added (mL)	Filtration Eff.	Inflow TS	Output TS	k (cm/sec) initial	k (cm/sec) DI	k (cm/sec) DI (2nd)
12	1,000	82.41%	0.14%	1.54%	$1.12x10^{-3}$	$1.13x10^{-3}$	$9.76x10^{-4}$
14	500	90.92%	0.37%	1.77%	$1.55x10^{-3}$	$4.21x10^{-4}$	
16	1,000	92.79%	0.48%	1.65%	$3.76x10^{-3}$	$1.93x10^{-3}$	$3.74x10^{-3}$
18	1,000	92.36%	0.46%	1.77%	$3.43x10^{-3}$	$4.80x10^{-3}$	$3.15x10^{-3}$

The third set of filter tests were run by using slurry collected from the T&T Site. This slurry was collected from the material headed for the geotextile tubes that were on site. This slurry had been treated with 20 ppm of polymer as well as the lime slurry. This set of tests used the same fabrics that the second set conducted with. The results for the third set of tests are shown in Table 10-13.

Table 10 : 20 ppm Polymer T&T GT500 Filtration Results

GT500 Data		Filtration	Slurry	Filter Cake	Hydraulic Conductivity		
Test #	Volume of DI Water Added (mL)	Filtration Eff.	Inflow TS	Output TS	k (cm/sec) initial	k (cm/sec) DI	k (cm/sec) DI (2nd)
23	1,000	91.05%	0.74%	2.89%	$6.98x10^{-4}$	$7.74x10^{-5}$	$4.84x10^{-5}$
24	1,000	92.08%	0.72%	1.95%	$6.19x10^{-4}$	$1.63x10^{-4}$	$6.06x10^{-5}$

Table 11 : 20 ppm Polymer T&T MD88 Filtration Results

MD88 Data		Filtration	Slurry	Filter Cake	Hydraulic Conductivity		
Test #	Volume of DI Water Added (mL)	Filtration Eff.	Inflow TS	Output TS	k (cm/sec) initial	k (cm/sec) DI	k (cm/sec) DI (2nd)
29	1,000	94.16%	1.15%	2.76%	$7.08x10^{-4}$	$5.78x10^{-5}$	$1.06x10^{-4}$
30	1,000	94.39%	0.89%	2.83%	$8.76x10^{-4}$	$7.61x10^{-5}$	$2.16x10^{-5}$

Table 12 : 20 ppm Polymer T&T 140NC Filtration Results

140NC Data		Filtration	Slurry	Filter Cake	Hydraulic Conductivity		
Test #	Volume of DI Water Added (mL)	Filtration Eff.	Inflow TS	Output TS	k (cm/sec) initial	k (cm/sec) DI	k (cm/sec) DI (2nd)
25	1,000	92.51%	0.75%	2.83%	$6.37x10^{-4}$	$8.13x10^{-5}$	$5.30x10^{-5}$
26	1,000	91.41%	0.74%	2.19%	$4.98x10^{-4}$	$5.73x10^{-5}$	$7.61x10^{-5}$

Table 13 : 20 ppm Polymer T&T 1100N Filtration Results

1100N Data		Filtration	Slurry	Filter Cake	Hydraulic Conductivity		
Test #	Volume of DI Water Added (mL)	Filtration Eff.	Inflow TS	Output TS	k (cm/sec) initial	k (cm/sec) DI	k (cm/sec) DI (2nd)
27	1,000	93.46%	0.75%	2.59%	$6.03x10^{-4}$	$5.89x10^{-5}$	$6.41x10^{-5}$
28	1,000	88.63%	0.75%	2.29%	$6.41x10^{-4}$	$1.08x10^{-4}$	$6.32x10^{-5}$

3.5 Discussion of Results

The results shown in tables 3-13 will be discussed in the following section. Evaluation is based on their filtration efficiency, hydraulic conductivity, and the change in total solids between the slurry and the filter cake. Each fabric will also be compared between each of the polymer amounts to assess how a polymer addition effects. Table 14 shows the average initial hydraulic conductivity, filtration efficiency, incoming total solids, and the filter cake total solids for each of the fabrics between the 2 polymer doses. In this table the values can be easily compared between the different polymer doses that were used. Where the addition of polymer is expected to decrease the hydraulic conductivity increase the filtration efficiency in the GT500 fabric and increase the total solid content in the filter cake after filtration is complete.

Table 14: Average Values from Column Filter Test Results

Material	Fabric	Hydraulic Conductivity (cm/s)	Filtration Efficiency	Incoming Total Solid	Filter Cake Total Solid
Omega No Polymer	GT500	$2.48x10^{-3}$	78.50%	0.78%	2.07%
	MD7407	$1.66x10^{-3}$	94.70%	1.27%	2.52%
	MD88	$3.66x10^{-3}$	91.10%	0.89%	1.98%
	1100N	$2.47x10^{-3}$	89.60%	0.36%	1.68%
	140NC	$4.26x10^{-3}$	91.70%	0.47%	1.73%
T&T 20 ppm Polymer	GT500	$6.59x10^{-4}$	91.60%	0.73%	2.42%
	MD88	$7.92x10^{-4}$	94.30%	1.02%	2.79%
	1100N	$6.22x10^{-4}$	91.05%	0.75%	2.44%
	140NC	$5.68x10^{-4}$	91.96%	0.75%	2.51%

3.5.1 Filtration

The filtration results from Table 4 and 5, which is the data for the two typar wick drain fabrics, show that the MD88 fabric is more consistent and has a better average filtration efficiency between all three tests. In Table 15 the filtration data that was collected after the tests that compare the results for the MD88 and MD7407 typar fabrics. Based off these results a decision to choose the MD88 wick drain in all future experiments and designs was made because of the

higher filtration efficiency and higher solids retention trapped in the filter itself (this is found based on the grams lost per unit area).

Table 15: Initial No Polymer Omega MD88 Typar vs MD7407 Typar Filtration Data

Test #	Fabric	AOS (mm)	% Retained	% Passing	Filtration Eff.	% Lost	grams lost per unit area (cm^2)
2	MD7407	0.23	92.41%	7.28%	92.72%	0.31%	0.1076
7	MD7407	0.23	97.00%	2.89%	97.11%	0.11%	0.0523
9	MD7407	0.23	94.17%	5.74%	94.26%	0.09%	0.0982
3	MD88	0.09	94.73%	5.17%	94.83%	0.10%	0.0804
5	MD88	0.09	95.84%	3.79%	96.21%	0.37%	0.0607
8	MD88	0.09	95.77%	4.21%	95.79%	0.03%	0.0750

The filtration efficiency results are consolidated in a box and whisker plot. For each of the fabric tested are shown in Figure 5. Important metrics show the inconsistent filtration efficiency range of the GT500 fabric w from 50-96%. The MD88 fabric is by far the most efficient with having majority of the tests being above 94% with one outlier point. The comparison of the two woven fabrics, 140NC and 1100N, shows that the 140NC is more accurate between all the tests taken with all the values being above 91%, and the 1100N had one test that was far below the average of 90%.

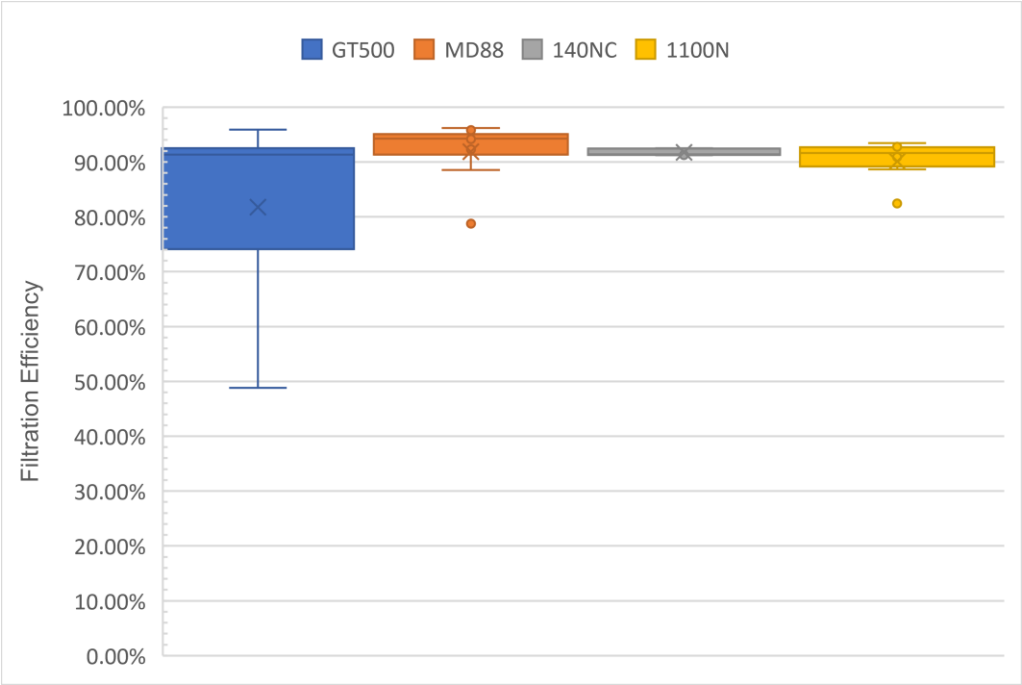

Figure 5: Box and Whisker Plot of Filtration Efficiency

3.5.2 Hydraulic Conductivity

From the testing it was shown that the hydraulic conductivity decreased with time for each fabric. The significant difference was noticed when comparing either the total solids of the material that was being tested and if the slurry was using polymer or not. The decrease in hydraulic conductivity with time is more noticeable when comparing the different polymer dosages tested. Figure 6 shows the hydraulic conductivity (log scale) vs time for tests 10, 13, and 15 which were from the No Polymer Omega Slurry using the GT500 fabric. This figure combines all the data from each of the tests in order to create a line of best fit Based on the figure it shows that the hydraulic conductivity is expected to decrease with time. The following figures were created using JMP Statistical Software© in order to create the line of best fits with the confidence interval.

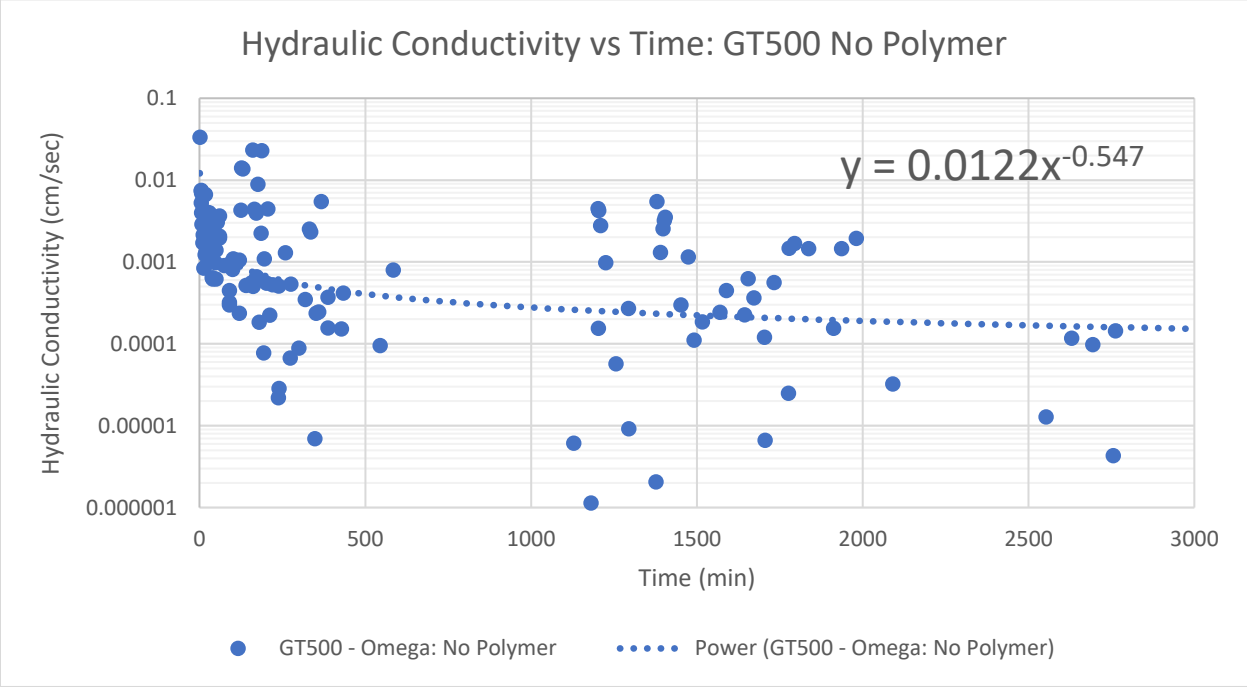

Figure 6: Hydraulic Conductivity GT500 with No Polymer Omega Sludge

Figure 7 shows the hydraulic conductivity (log scale) vs time for tests 23 and 24 which were from the 20 ppm polymer dosed T&T Slurry using the GT500 fabric. This figure has both tests data combined in order to create a logarithmic line of best fit. This figure also shows that the hydraulic conductivity is expected to decrease with time. In comparison between Figure 6 and 7, the hydraulic conductivity decreases at a faster rate when polymer is used in the slurry. Where

Figure 6 decreases from $1x10^{-2}$ cm/s to $1x10^{-3}$ cm/s and Figure 7 decreases from $1x10^{-3}$ cm/s to $5x10^{-4}$ cm/s. The test duration for the polymer dosed tests was significantly longer than the raw slurry where Figure 6 ran for almost 3,000 minutes and Figure 7 ran for almost 15,000 minutes with is 5 times as long.

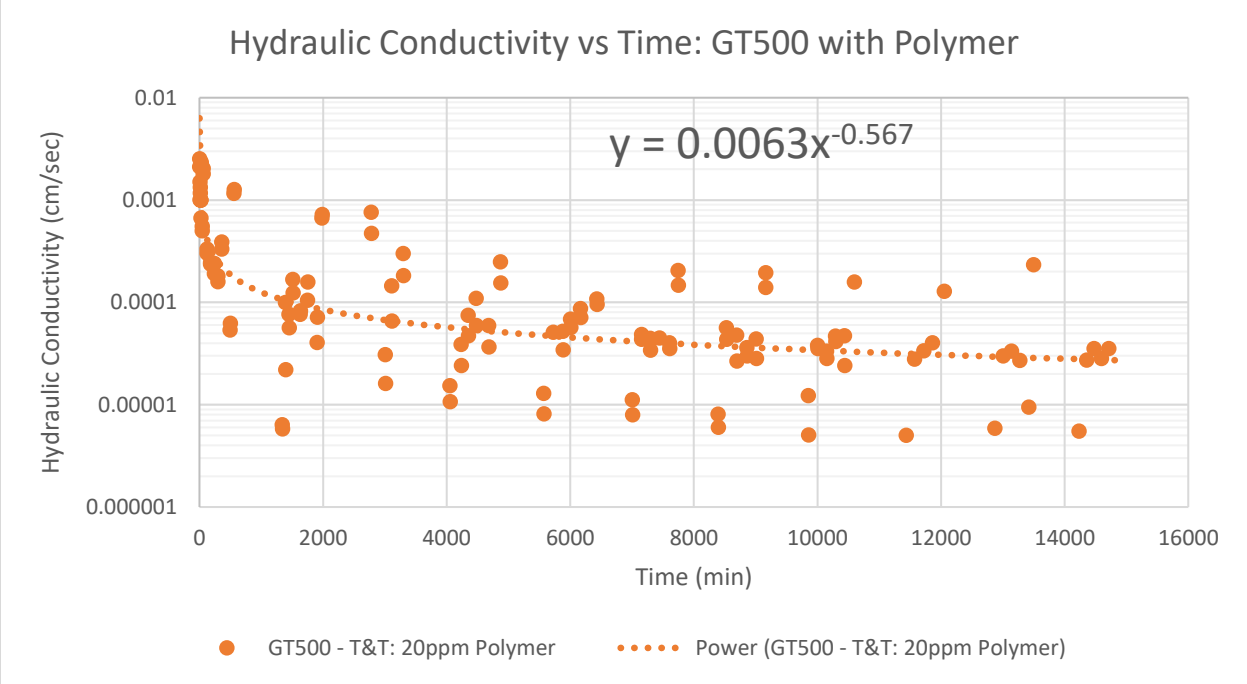

Figure 7: Hydraulic Conductivity GT500 with 20 ppm Polymer T&T Sludge

Figure 8 shows the hydraulic conductivity (log scale) vs time for test 27 which was done using the 1100N nonwoven fabric using the 20 ppm polymer T&T slurry. This test follows the same trend from Figure 7 where the decrease in hydraulic conductivity with time is the same and then the duration of the test is also similar. Based on the comparison of the Figure 7 and Figure 8 it seems that the fabric used does not play a factor into the change in hydraulic conductivity. The fabrics are dependent on the filtration efficiency and solids retained based on the AOS of the fabric.

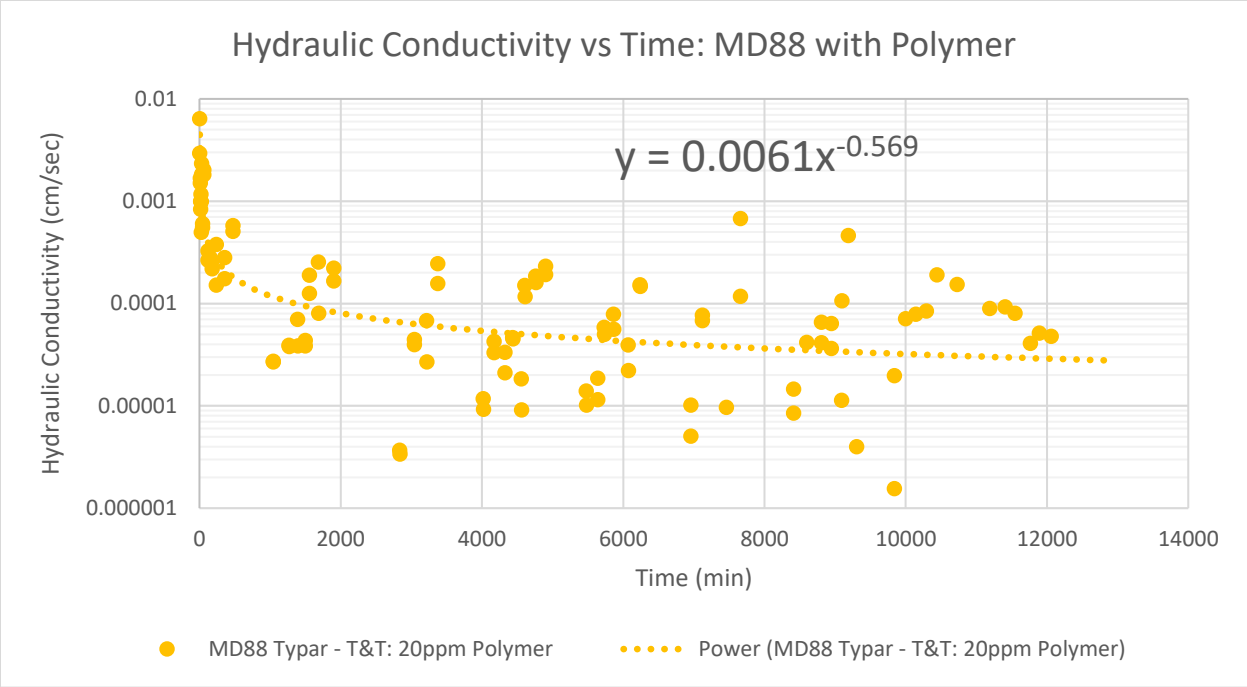

Figure 8: Hydraulic Conductivity 1100N with 20 ppm Polymer T&T Sludge

More plots for hydraulic conductivity vs time are listed in Appendix A where the lines are separated between the different filling cycles. In these plots all the different test's lines are independent.

3.5.3 Total Solids

The total solids in the material were measured for each test at two separate times. The first time was to determine the total solids of the incoming slurry, this was done by averaging three samples taken from a bucket filled with AMD slurry. The second time it was collected was from the filter cake once the filtration tests was complete, this was done by taking the average TS% from the top and the bottom of the filter cake. Figures 9 and 10 are two box and whisker plots which show the difference in total solids between the incoming slurry and the filter cake. Figure 9 shows the change when using the No Polymer Omega AMD Slurry and Figure 10 shows the change when using the 20 ppm polymer T&T AMD Slurry.

For Figure 9 the average total solids for the slurry is 0.76% which than increases to an average of 1.99% for the filter cake. In Figure 10 the average total solids for the slurry is 0.81% and the average for the filter cake is 2.54%. This means that the incoming total solids is very similar between the 2 samples of AMD Slurry but with the introduction of polymer the filter cake is

expected to increase in the total solids percentage. The no polymer Omega slurry has an increase in total solids by 162% and the 20 ppm polymer T&T slurry increases by 214%

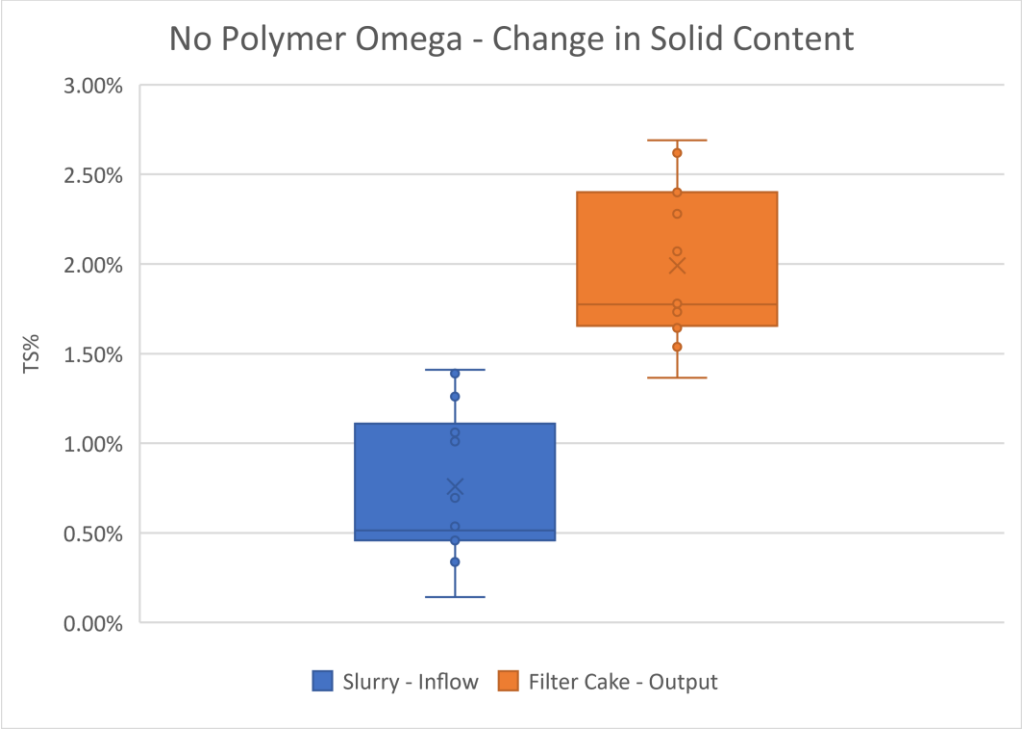

Figure 9: Raw (no polymer) Omega Change in Solid Content from Slurry to Filter Cake

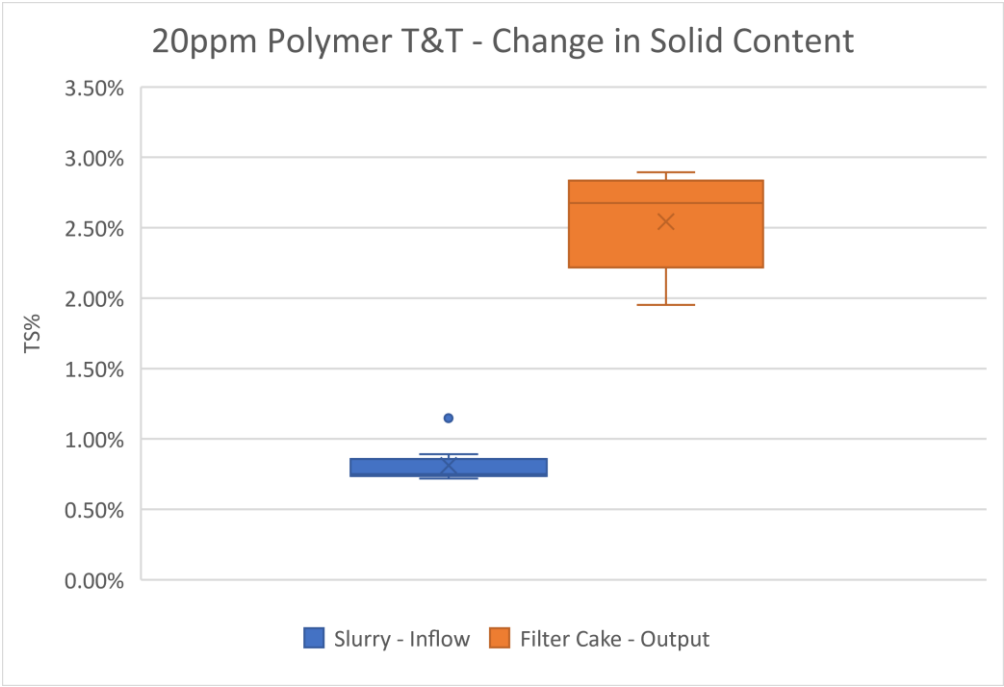

Figure 10: 20 ppm polymer dose T&T Change in Solid Content from Slurry to Filter Cake

3.6 Filtration Test Findings

This study tested five different geotextile fabrics and two different AMD sludges. The geotextile fabrics and AMD sludges were evaluated to determine the filtration efficiency and hydraulic conductivity changes in order to select the optimum fabric and optimum geotextile for lateral drainage applications. Preliminary findings tend to indicate that:

1) With and without polymer the 1100N nonwoven fabric has the highest filtration efficiency
2) Without polymer the MD88 Typar fabric has the higher filtration efficiency (95.61% vs 94.7%) but has a lower hydraulic conductivity which means the fabric clogs faster than the MD7407 Typar fabric
3) The amount of polymer affects the hydraulic conductivity. The 20 ppm T&T material's hydraulic conductivity stabilized at $3x10^{-5}$ cm/s and the Raw (no polymer) Omega material stabilized at $3x10^{-4}$ cm/s
4) The systems (filter cake + geotextile) hydraulic conductivity was found to be independent of the geotextile used. This implies that the filter cake hydraulic conductivity controls drainage. The drainage process requires that the geotextile filter is developed, and a stable filter cake is developed.
5) The Apparent Opening Size (AOS) of the fabric had an effect on the clogging of the fabric. Where fabrics with a smaller AOS (MD88) clogged faster than those with a larger AOS (GT500). This process impacts whether the fabric blinds-off drainage flow or whether a stable filter cake is formed. For the lateral drainage, the prefabricated vertical drain and typar fabric blinds-off and does not develop a lower hydraulic conductivity filter before the larger AOS geobag fabric does. The typar fabric blinding diminishes drainage (10X) compared to the nonwoven geotextiles (1100N and 140NC).

3.7 Design Recommendations

Considering the performance and analysis of the column tests running the two wick drain typar fabrics (MD88 and MD7407), it is recommended that the MD88 fabric be used when constructing the prototype geotextile bags intended to test field scale dewatering. The MD88 typar fabric has a higher filtration efficiency, which is due to its smaller AOS. The results that were used to produce this decision are taken from Tables 4, 5 and 15. A testing alternative is

install the MD88 as the internal lateral drain and have the drain wrapped by 1100N fabric to limit the clogging, promote filter cake formation, and develop a stable drainage filter.

From the performance and analysis of the column tests running the non-woven fabrics (1100N and 140NC), it is recommended that the 1100N fabric be used in the filtration and dewatering in other geotextile bag designs. Between the two nonwoven fabrics (1100N and 140NC) the 1100N showed better filtration capabilities when running the lime dosed slurry. This is done by removing the outlier with the filtration efficiency is 82% when looking at Table 9. By removing this outlier, the rest of the data shows that the filtration efficiency is higher than the 140NC fabric.

When running the tests, the filtration efficiencies varied and were generally more efficient when the incoming slurry total solids was greater than 0.75% when compared to the tests that had the total solids in the slurry under 0.75%. Therefore, the optimum conditions to have the most efficient treatment is to have the total solids of the slurry to be greater than 0.75%. To catch the solid particles more effectively and there will be a larger filter cake.

4.0 Moisture Distribution Test Methods

The purpose of this testing was to determine the moisture distribution throughout geotextile tubes that are in the field at the West Virginia Department of Environmental Protection (WVDEP) (T&T and Omega) sites. This testing was to determine dewatering distributions and the total solid layering. The geotextile tubes are the most common method for dewatering large volumes of sludge, understanding the total solid distribution inside the bags can help to develop new designs to promote more efficient inside dewatering. The geotextile tubes have AMD slurries pumped into them and then allowed to dewater over time, so by collecting field samples at different times the dewatering efficiency can be shown This study investigates the flow of solids inside the geotextile tubes by collecting samples from inside tubes from different depths obtained from the tube's injection ports.

Once the tests have been completed for each of the tubes an illustration of total solids percentage will be created to show distribution inside the tubes. These illustrations will show the layers based on the different pumping cycles and the hotspots of where the higher amount of solids are. The illustrations will also show the flow of moisture inside the tubes that can show where majority of the water flows to and where it gets trapped.

4.1 Objective

The purpose of the total solids distribution testing will be accomplished by collecting samples from the side of the geotextile tubes at different depths and across different distances at one cross section. The testing will be done following ASTM D2216 which is the Standard Test Methods for Laboratory Determination of Water (Moisture) Content of Soil and Rock by Mass. Following this ASTM will produce the moisture content for each sample that was collected and by using the total solids percentage from the sample a current model will be created that presents the current distribution of moisture based on the different cross sections that were selected.

To accomplish the purpose the following objectives will be performed:

- 1. Build a Sampler
- 2. Obtain Samples
- 3. ASTM Tests
- 4. Reduce Data

- 5. Build Figures

4.2 Testing Procedure

In situ sludge samples were collected from different depths within the geotextile bag by using a 2 in pvc pipe that had 9-10 cm holes set at 10 cm increments. Five to six different samples for each hole dug in the geotextile tube were taken. The PVC pipe was constructed by cutting a semicircle hole in the pvc pipe on one side and having a thin slit cut parallel to the flat edge of the semicircle. A piece of aluminum was used to scoop the sludge into the opening in the pvc pipe. Figure 11 is the second sampler that was constructed with a longer pipe section to allow for more scoops/holes.

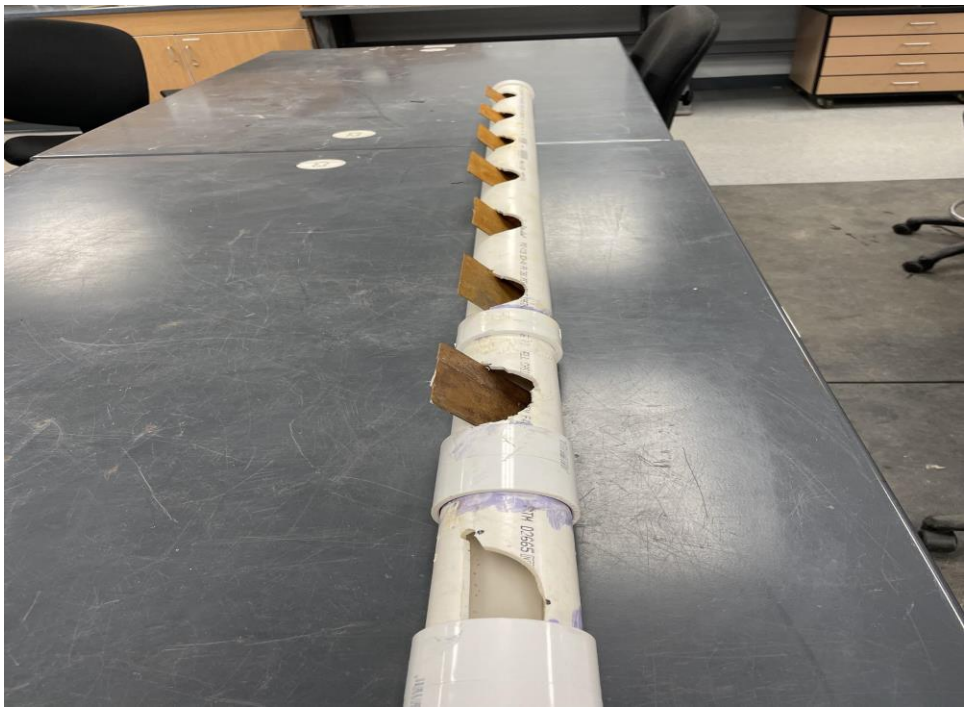

Figure 11: Version 2 6ft Sampler with 7 holes (Source: Tyson 2022)

The testing method to determine the moisture contents was done following the ASTM D2216-19: Standard Test Methods for Laboratory Determination of Water (Moisture) Content of Soil and Rock by Mass. Each test was run using triplicate testing and then determining the average value of the 3 for the reported value. The specific gravity was also determined for each of the cross sections that were being tested. This test was done by following the ASTM D854-14: Standard Test Methods for Specific Gravity of Soil Solids by Water Pycnometer.

4.2.1 Testing

Materials Needed:

- Obtain 6 tubes (for each dig being conducted) with a sealable lid to transport samples from field back to the lab
- Obtain a spoon or flat edge spatula
- Large metal spoon
- Constructed Sampler
- 5-gallon buckets (1 for each cross section)
- Duct Tape
- Sharpie
- Wooden 2x4
- Rubber Mallet/Hammer
- Scissors
- Cutting Knife
- Metric Tape Measure
- Slip Wrench

Collection:

1) Determine the field geotextile tube that will be collected from and count the number of bags from the far wall down to the one chosen. With the selected bag choose which center port or cross section will be collected from.
2) With the chosen bag and cross section selected measure from the edge of the bag closest to the open edge. Also measure the distance from the center port to the sides of the bags.
3) Starting from the center port push down the sampler until it cannot be pushed down anymore. From here take the 2x4 and the rubber mallet and drill down as far as possible or until all the holes are submerged. Shown in Figure 12 is how the board should be used.

Figure 12: Moisture Distribution Sampler with 2x4 board (Source: Tyson 2022)

4) With the submerged sampler in the sludge start twisting in the direction of the sampler's openings, as to scoop the sludge in with the aluminum slices. Rotate the sampler until there is hardly any friction resisting motion.

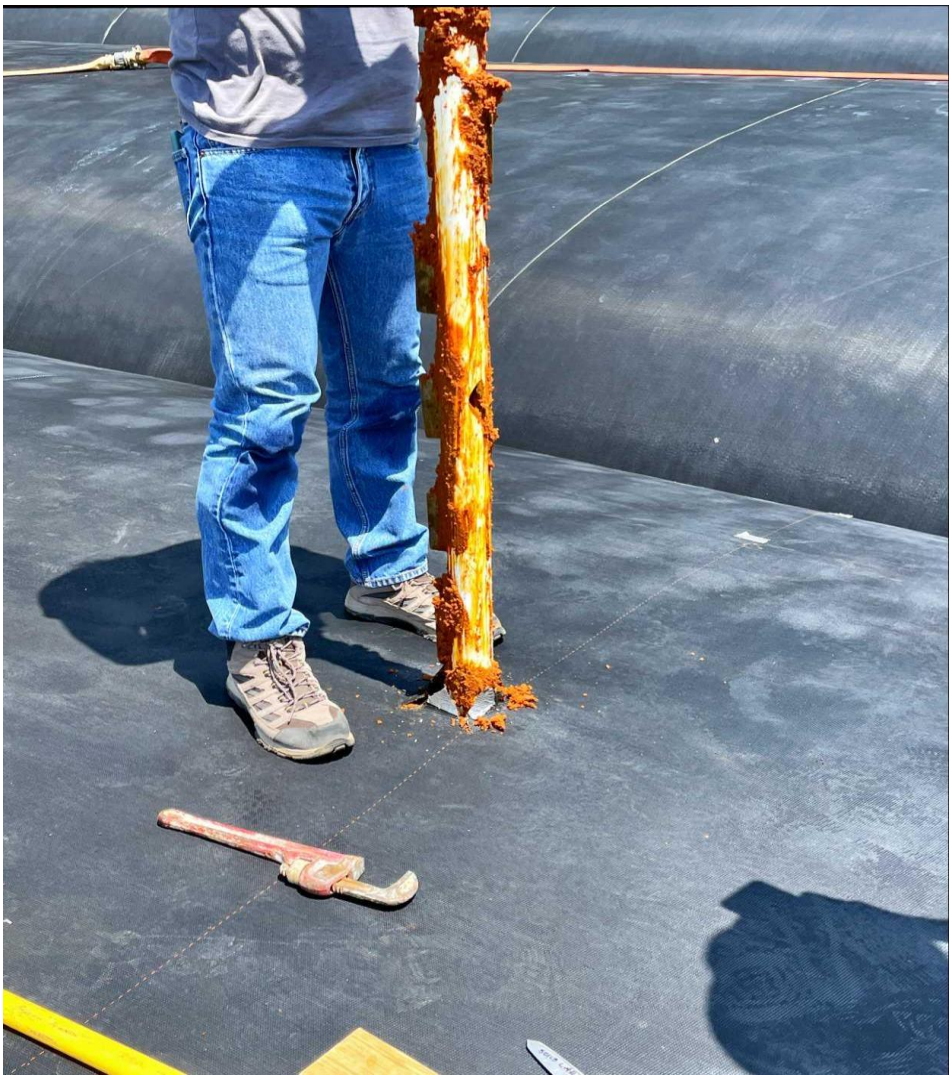

Figure 13: Removal of Sludge Sampler (Source: Tyson 2022)

5) Remove the sampler from the hole, carefully not to lose any samples. Figure 13 illustrates the sampler should be removed. Then with the spoon/spatula scoop the sludge from the blades and in the hole and deposit into labeled tubes depicting the dig, the hole number, and the geotextile tube being tested on.

Figure 14: Removed Sampler read for Sample to be Collected (Source: Tyson 2022)

6) Before moving on to the next sample location, the sampler should be cleaned of any excess material as to not cross contaminate into other holes or bags.
7) Continue to the next hole in the cross section by measuring an even distance from the center port (even distance meaning where you could do 3 or 4 holes across the cross section). Using the knife to cut into the geobag, cut a wide enough hole (create a cross in the bag and fold the flaps upwards) to allow for the sampler to fit inside. Follow the same steps as 3-6 for this hole. After the sampler has been removed using the duct tape on the slits in the geobag to close the hole.
8) Repeat Step 7 for each of the holes in the cross section.
9) Before leaving the geobag, collect enough material to fill about a third of a 5-gallon bucket to determine the specific gravity

Testing:

Moisture Content:

1) When back in the lab take out 3 moisture content tins for each of the sample tubes that were filled.
2) Taking note of the label on each of the moisture content tins, write down the name and the empty weight of each.
3) Fill each moisture content tin with about a third of the sample that was collected from the site. Weigh the filled moisture content tin and place into the oven at 110 degrees Celsius for at least 16 hours.
4) With the dried samples take them out of the oven and weigh the dried weight before calculating the moisture content for each of the tins.

Specific Gravity:

1) Take some of the material from the bucket and place into a large bowl to place into the oven. This is done due to the high moisture content of the material.
2) Once the material is dried take it out of the oven and measure about 50grams of dried material and place to the side to be used in the specific gravity testing
3) Grab an empty pycnometer and grab the empty weight. Fill the pycnometer with deionized water and start deairing it at the vacuum pumps.
4) With a full pycnometer of deaired water, grab the full weight before emptying into a 600-1,000 mL beaker.
5) With the full beaker place a thermometer to determine the temperature of the deaired water.
6) While collecting the temperature start pouring the oven dried material into the pycnometer using a funnel and a squirt bottle to make sure all material goes into the pycnometer.
7) Pour some deaired water into the pycnometer, be sure not to fill all the way to the top. Swirl the pycnometer before hooking it up to the vacuum pump. This step should be done until the water reaches the line in the spoke of the pycnometer.
8) Weigh the filled pycnometer and then pour into a dry bowl before being placed into the oven. This is done to determine the mass of the soil.

9) After weighing the dried bowl, place all the data into the calculations to determine the specific gravity for the material in the specific cross section.

4.3 Results

The moisture content and total solids percentage results for the sampler tubes tested are listed in Appendix A with Table 16 shown as a reference indicating how the data is further reported. The remainder of the data are organized in Appendix B by the center port and then to the right in that cross section. For the bags with full cross sections tested the specific gravity results are shown in Table 17. Out of the bags sampled there were 2 samples taken from a center port only (Bag 5 and 11), 3 bags with 1 cross section sampled (Bag 6, 7, and 9), and 1 bag with 2 cross sections sampled (Bag 11) which are shown in Figures 16-26.

Table 16: Omega Geobag 11 Center Port

Distance from Surface (cm)	**Moisture Content**	**Total Solids**
0	97.51%	2.49%
9		
20	96.01%	3.99%
29		
40	96.33%	3.67%
49		
60	95.39%	4.61%
69		
80	95.20%	4.80%
89		

Table 17: Omega Geobags Specific Gravity

Specific Gravity	Bag 6	Bag 7	Bag 9	Bag 11
Mass Pyc. (g)	160.3	168.3	159.5	160.6
Mass Pyc + Water (g)	657.7	666.3	660.0	658.0
Calibration Temp (Degrees C)	21.0	20.2	24.0	19.8
Density @ Cal. Temp (g/mL)	0.997	0.998	0.997	0.998
Calibrated Vol (mL)	498.40	498.92	501.84	498.27
Mass Pyc. + Water @ Test Temp (g)	657.7	666.3	660.0	658.0
Mass Pyc + Water + Soil (g)	690.01	697.68	691.00	690.10
Mass Soil (g)	49.43	48.87	48.90	49.50
Volume Pyc (mL)	498.40	498.92	501.84	498.27
Test Temp (Degrees C)	21.0	20.2	24.0	19.8
Density Water @ Test Temp (g/mL)	0.997	0.998	0.997	0.998
Specific Gravity	2.89	2.79	2.73	2.84
Temp. Coeff (K)	0.998	0.998	0.998	0.998
Specific Gravity @ 20°C	2.88	2.79	2.73	2.84

4.4 Discussion

4.4.1 Moisture Distribution

The moisture distribution throughout each of geobags the points were transposed into AutoCAD. For synthesis, the first two tests that were conducted only 1 dig sample was done. These tests were done on a dry bag (Bag 5) and in a new bag that was still being pumped into (Bag 11). The cross-sectional distribution models are shown in Figure 15 and 16. When looking at each of the cross sections the black rectangles indicate the sampler hole spacing and where the sludge was collected.

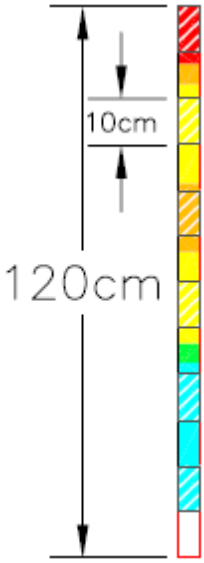

Percent Total Solid Ranges			
Range #	Minimum TS	Maximum TS	Color
1	5.00	5.25	
2	5.25	5.50	
3	5.50	5.75	
4	5.75	6.00	
5	6.00	6.25	
6	6.25	6.50	
7	6.50	6.75	

Figure 15: Omega Geotextile Bag #5 – Sampled 5/23/22

The spacing in the 5th geotextile bag is in 10 cm increments with the data being collected using one of the early iterations of the sampler design. The model shows that the bag has a higher TS% closer to the top of the bag. With this being an older bag, it has had more time than other bags to be able to dewater and have the sun evaporate any moisture near the top of the bag. It can be inferred since this was a relatively old bag that there was limited moisture movement out of the bag but it all pools near the bottom along the formed filter cake.

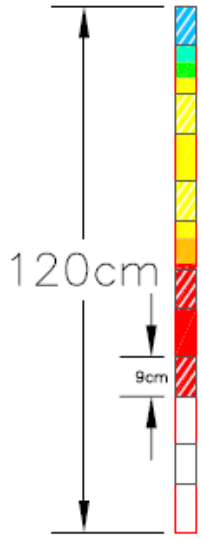

Percent Total Solid Ranges			
Range #	Minimum TS	Maximum TS	Color
1	1.00	1.50	
2	1.50	2.00	
3	2.00	2.50	
4	2.50	3.00	
5	3.00	3.50	
6	3.50	4.00	
7	4.00	4.50	
8	4.50	5.00	

Figure 16: Omega Geotextile Bag #11 – Sampled 6/03/22

The data for the 11th geotextile bag has 9 cm holes because it was using the 2nd iteration of the sampler design. The data show that the geotextile bag is wetter at the top than at the bottom of the bag. The difference between bag 11 and bag 5 is that bag 11 was still being pumped into so the viscosity of the sludge allowed for the solids to flow to the bottom of the bag easier. This is because the bags were still being pumped into so all the fresh sludge was at the top of the bag and the older sludge was at the bottom which had a longer time to dewater. When collecting the material from this bag it was the 2nd newest bag and had been pumped into since the first of March 2022, and the material was collected the third of June 2022.

The data collected from the 6th, 7th, and the 9th Geotextile bags at the Omega site had enough information to create a plot of the moisture distribution throughout a cross sectional area. The plot for the moisture distribution is shown in Figure 17 and Figure 18 for bag 7 and 9, respectively. Figure 19 is the legend used for both models. Figure 20 shows the moisture distribution model for bag 6 with Figure 21 showing the corresponding legend similar to the other two plots the black rectangles indicate where each of the holes in the sampler were and then the red rectangles indicate where the sampler was inserted for each dig.

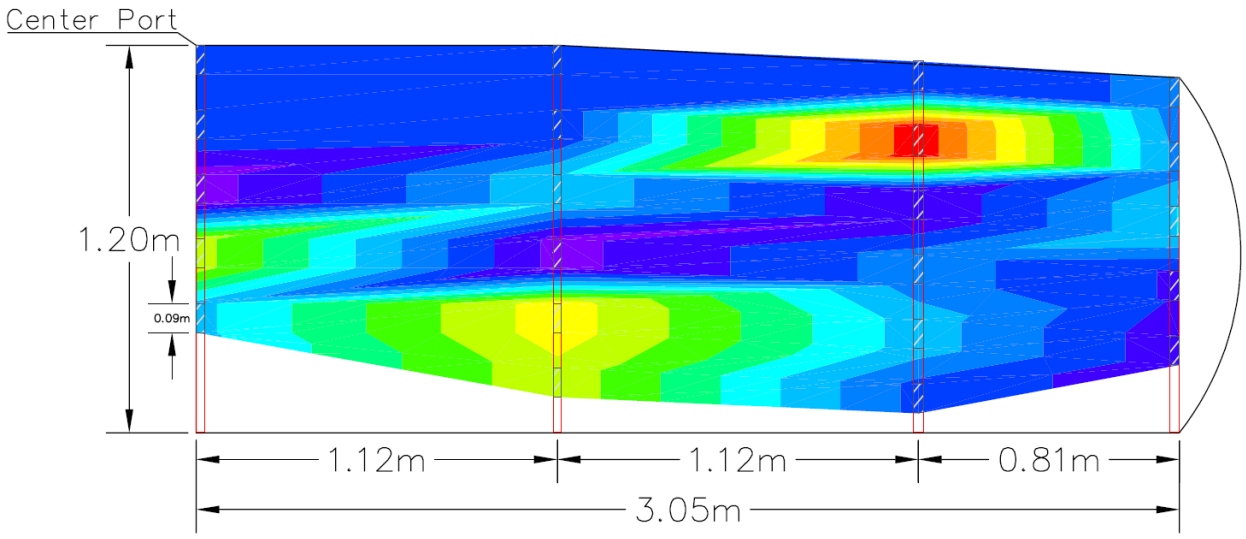

Figure 17: Total Solids Distribution Omega Geotextile Bag #7 – Sampled 6/08/22

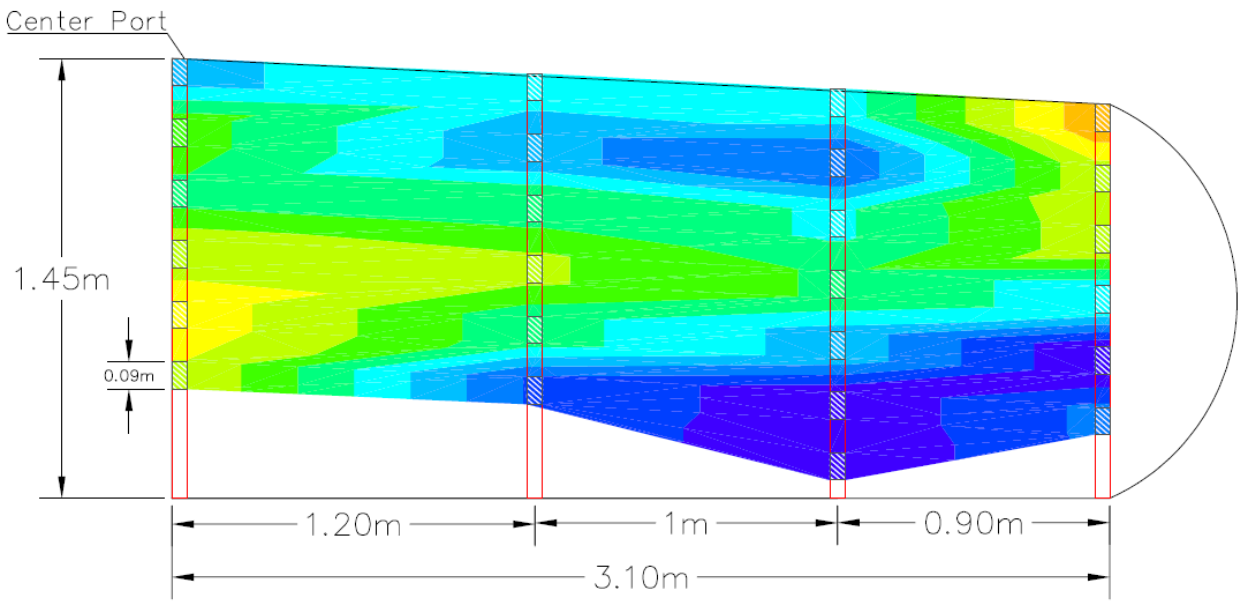

Figure 18: Total Solids Distribution Omega Geotextile Bag #9 – Sampled 9/09/22

Percent Total Solid Range			
Range #	Minimum TS	Maximum TS	Color
1	5.00	5.50	
2	5.50	6.00	
3	6.00	6.50	
4	6.50	7.00	
5	7.00	7.50	
6	7.50	8.00	
7	8.00	8.50	
8	8.50	9.00	
9	9.00	9.50	
10	9.50	10.00	
11	10.00	10.50	
12	10.50	11.00	
13	11.00	11.50	

Figure 19: Omega Geotextile Bag #7 and #9 TS Legend

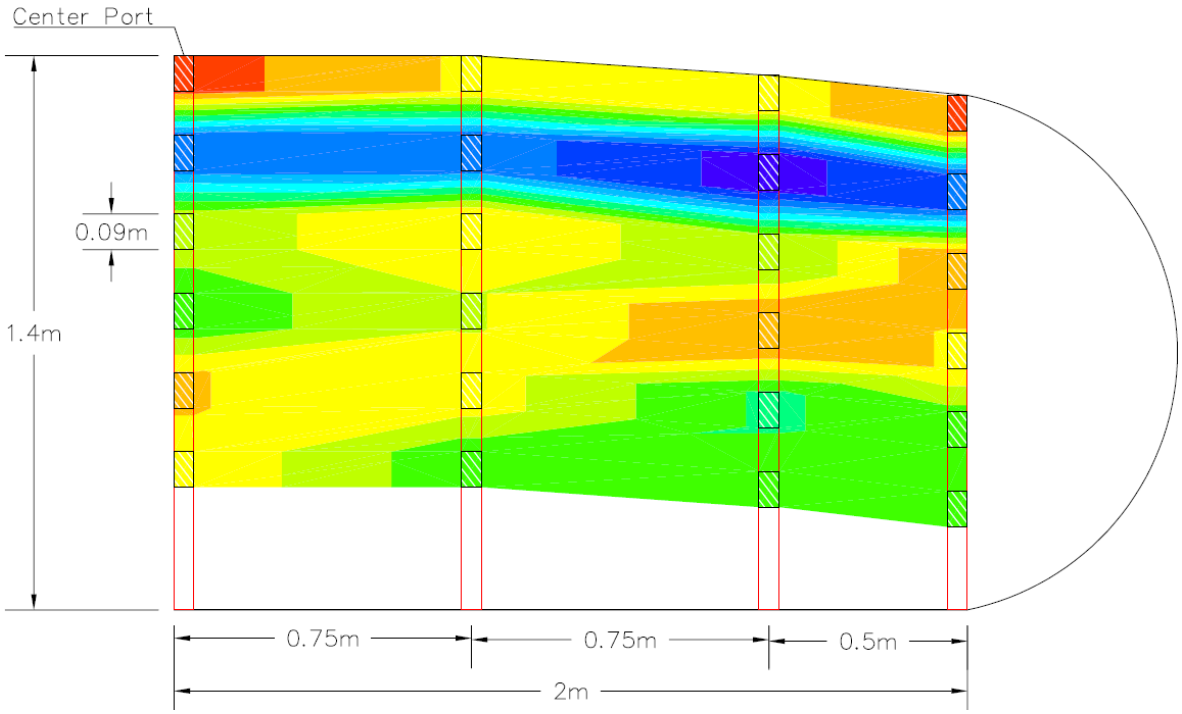

Figure 20: Total Solids Distribution Omega Geotextile Bag #6 – Sampled 1/17/23

Percent Total Solid Range			
Range #	Minimum TS	Maximum TS	Color
1	4.50	4.75	
2	4.75	5.00	
3	5.00	5.25	
4	5.25	5.50	
5	5.50	5.75	
6	5.75	6.00	
7	6.00	6.25	
8	6.25	6.50	
9	6.50	6.75	
10	6.75	7.00	
11	7.00	7.25	
12	7.25	7.50	

Figure 21: Omega Geotextile Bag #6 TS Legend

With the 6th, 7th, and 9th bag all getting 4 digs across half the length of the bag a plot was created to show how the moisture distributes throughout the axisymmetric cross section. When looking at the plot in Figure 17, there are layers developed by the different filling cycles. The shape of these layers are in a similar shape has a parabola, where the bottom of the parabola is in the center and then arcs up towards the top edges. The moisture profile is not uniform this may be a result of high variability of the polymer dosage that is used and the different AMD treatment flow rates. When comparing the 7th bag (Figure 17) and the 9th bag (Figure 18), there are zones that have an elevated zone when looking at the total solids. When comparing the 7th and 9th bags, they are not uniform where the top of the 9th bag has more solids than the 7th bag. This may be due to inconsistencies in polymer addition, filling cycles, and the material coming to the site. When comparing the 6th bag (Figure 20) to the 7th and 9th bags (Figure 17 and 18 respectively), the 6th bag has different layers and average total solids than the other 2. This bag is wetter than the other 2, which could be different variables involved. These variables could be different weather and different time of year, where the 7th and 9th bag were collected in the summer and the 6th bag was collected in the winter.

After comparing how the moisture and TS% distribute between three different bags, the test objective advanced to assess the moisture profile within a single bag. To answer this question samples were collected from one of the geotextile bags at two different points along the length of the bag. Similar to the other cross sections each had 4 digs across half of the bag to create the model. The cross sections were taken from Omega Geotextile bag 11, which is also a bag that had been tested back in June 2022 but only material was taken from the center port. This geotextile bag was placed in March of 2022 with this sampling occurring on 2 November 2022. This bag was last filled in October of 2022prior to the sampling as well as that all pumping into the bag did not take place from either port that sample was taken from (all pumping took place from Cross Section C, see Figure 25 below). Figure 22 shows the moisture distribution for Cross Section A and Figure 23 shows the moisture distribution for Cross Section B with Figure 24 providing the legend for both cross sections.

One thing to compare from the Cross Section B from Bag 11 is to the singular dig shown in Figure 16 above. The sampling from the center port is the same region just 3 months apart. It

shows that there is a significant change in the solids content in this region over time going from a range of 3-5% to a range of 4-6%.

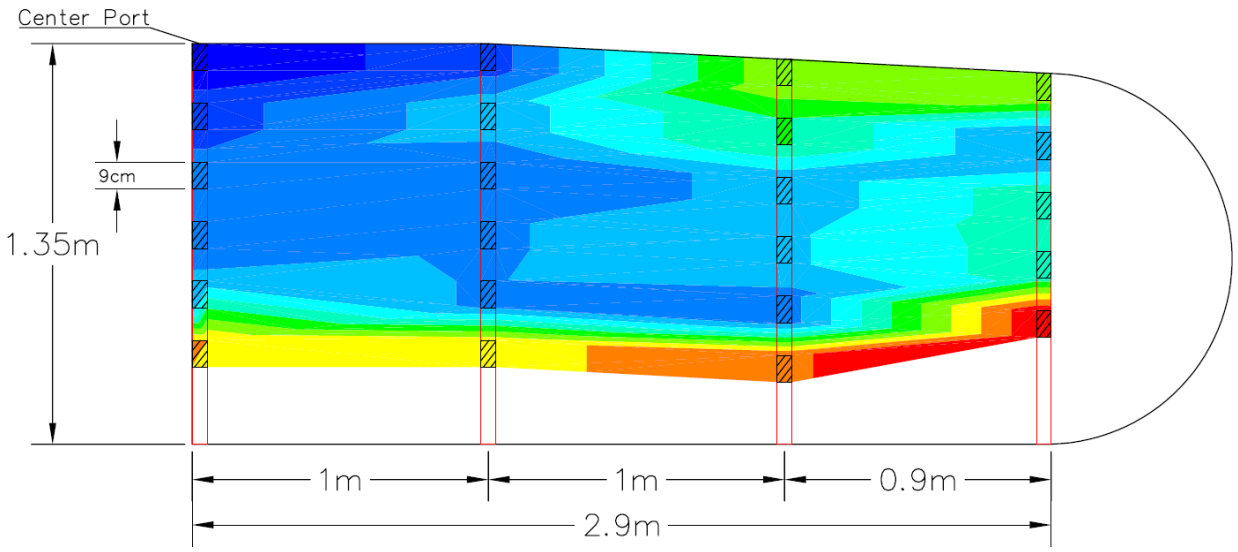

Figure 22: Total Solids Distribution Omega Geotextile Bag #11 Cross Section A – Sampled 11/02/22

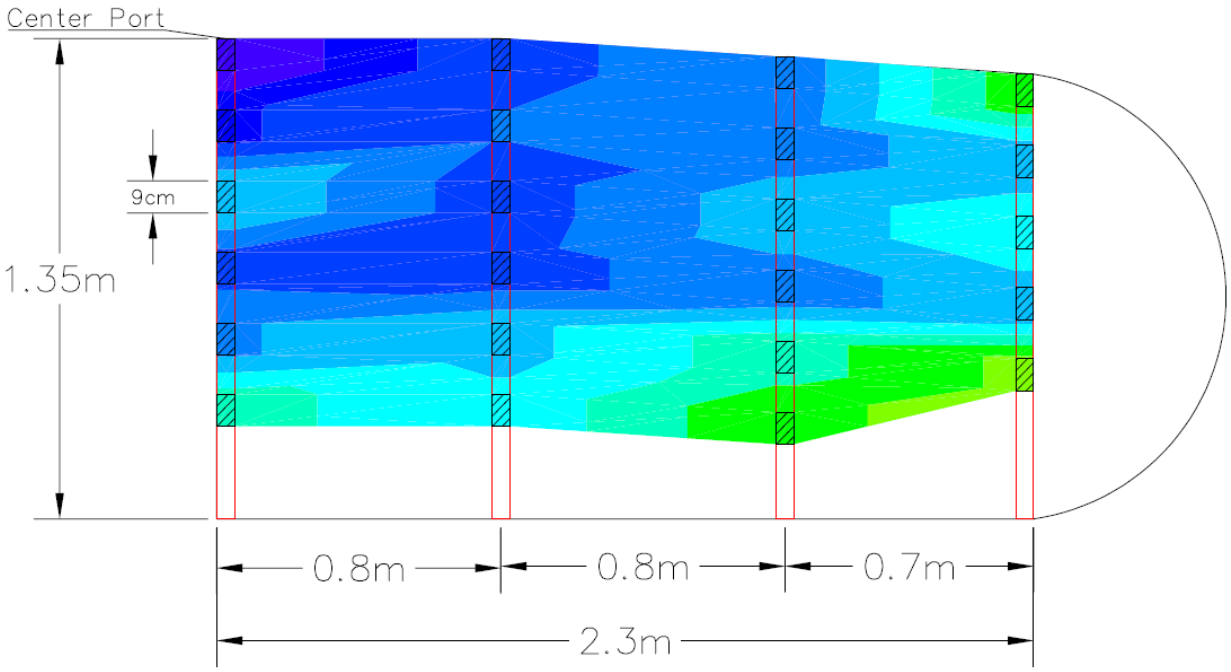

Figure 23: Total Solids Distribution Omega Geotextile Bag #11 Cross Section B – Sampled 11/02/22

Percent Total Solid Range			
Range #	Minimum TS	Maximum TS	Color
1	4.00	4.25	
2	4.25	4.50	
3	4.50	4.75	
4	4.75	5.00	
5	5.00	5.25	
6	5.25	5.50	
7	5.50	5.75	
8	5.75	6.00	
9	6.00	6.25	
10	6.25	6.50	
11	6.50	6.75	
12	6.75	7.00	
13	7.00	7.25	

Figure 24: Omega Geotextile Bag #11 TS Legend

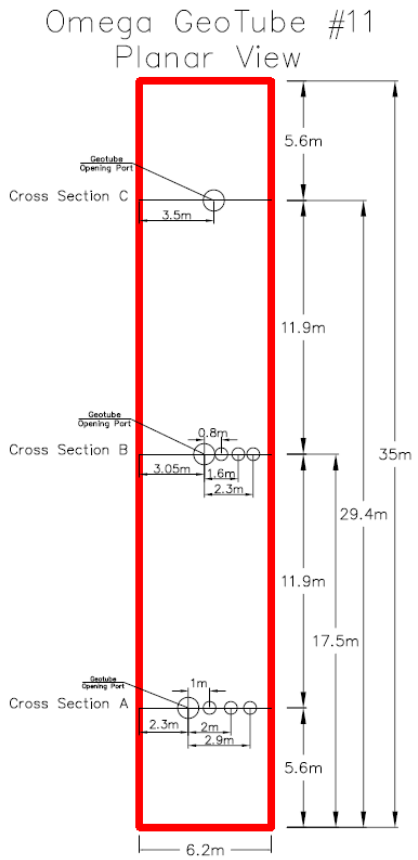

Figure 25: Planar View of Omega Geotextile Bag #11

The coring layout is illustrated in Figure 26 on a planar view of the 11th Geotextile bag, which was created to show where each of the ports are situated and the distance from the edge the samples were cored.

4.4.2 Specific Gravity

Besides the moisture content that was collected the specific gravity was also collected by getting a large sample of sludge from each bag. This was because of the low solids content of the material and the necessity of about 50grams of solids to run Specific Gravity Tests following the ASTM D854. The data for the bags specific gravity tests are shown in Table 17 above. A more condensed table showing the bags number, date the sample was collected, and the bags specific gravity are shown below in Table 18. The significance of the specific gravity is in correlation with how most soils fall between the range of 2.65 and 2.8 with the large the specific gravity the finer the soil. With the average between the four bags being 2.81. In this case bag 6 has the finest soil particles and bag 9 has the coarsest soil particles.

Table 18: Specific Gravity Consolidated Table

Bag #	Date Sample Collected	Specific Gravity
6	1/17/23	2.88
7	6/8/22	2.79
9	9/9/22	2.73
11	11/2/22	2.84
Average		2.81
Standard Deviation		0.056

4.5 Moisture Distribution Findings

This testing was conducted in order to determine the moisture and total solids distribution throughout geotextile tubes that are in the field. The bags that were selected were based on the pumping schedule that was being conducted at the AMD treatment site where the samples were collected. The goal was to collect samples from differently aged bags. The first tests that were conducted only had 1 sample per bag in order to figure out what was being tested for and what type of samples we wanted to collect. These tests provided how the distribution looks in the vertical direction only and where the moisture is expected to pool in the center of the bags. Which the older of the bags had more solids at the top and the newer bag had more solids at the bottom. The next set of tests were conducted to compare the distribution of moisture between

different bags. These tests showed a cross sectional area of where the sample was collected. Based on these profiles in Figure 18, 19, and 21 there is inconsistent flow trends. Where none of the three bags are similar in the layering of material and inconsistent in where majority of the solids pool together. The final test was conducted to compare the distribution within a single bag. These profiles in Figures 23 and 24 are similar in their layering because of where in the bag the sample is pumped.

The significant findings from this testing indicate:

1) There is no clear trend in the moisture profiles that indicate preferential sludge dewatering
2) There are no preferential drainage paths which indicate there are no clear placement of the lateral drains
3) Moisture within the geotextile tubes have to do with the use of a polymer, the polymer dose, the injection time, and the tube's age.
4) It is not possible to differentiate the zones of high polymer or low polymer within the geotextile tubes

The profiles that were created in this section will be used to be compared against in the next section, where numerical models will be created to create flow paths of how moisture is expected to flow in the material and out the geotextiles.

5.0 Finite Element Modeling

5.1 Purpose and Scope

The purpose finite element modeling is to mathematically predict the moisture movement under saturated and unsaturated flow conditions and how the use of the geotextile liner promotes flow within the geotextile tube. The models will be created using the data that was collected in laboratory testing in order to simulate the moisture movement when pumping in new material into the geotextile tube. The models that are created will be done by using data from the column filtration testing in Section 3 to analyze and compare with the field moisture tests in section 4 this will compare the modeled flow versus the field slurry fillings. The Plaxis 2D modeling software will be used for this research.

5.2 Objective

The objective of the finite element modeling is to build a model that predicts the moisture movement inside of a geotextile lined bag. The predictive numerical models will be constructed based on input lab variables collected from the previous sections. The predicted models will be compared against in the field profiles.

5.3 Numerical Modeling

A steady-state 2-dimensional model was created using Plaxis 2D Groundwater, which is a finite-element software for 2D analysis of deformation and stability in geotechnical and rock mechanics. The groundwater software module was used for the analysis for a flow of water in saturated and unsaturated soils. Groundwater allows for modeling dewatering in either a steady-state model or a time-dependent (transient) model. Using Plaxis to model flow in saturated soil follows Darcy's Law in which the rate of water flow through a soil mass is proportional to the hydraulic gradient. The flow for soil in an unsaturated state applies a mathematical function relating hydraulic conductivity to the soil saturation.

5.3.1 Materials Properties

The model is comprised of the input slurry material which was collected from a WVDEP site that was treating AMD. When running through oven-dried material through the ASTM D6913 (Standard Test Methods for Particle-Size Distribution (Gradation) of Soils Using Sieve Analysis) for grain size classification, the material was found to be a silt. A woven geotextile called GT500

was used and has the properties listed in Table 19. The properties that are present are the apparent opening size and the flow rate for the geotextile as well as the ASTM that are used in order to determine those values.

Table 19: Finite Element Modeling Woven Geotextile Properties

Mechanical Property	ASTM Test Method	GT500
Fabric type		Woven
Apparent Opening Size (AOS) (mm)	ASTM D4751	0.425
Flow Rate (L/min/m^2)	ASTM D4491	815

The next set of data is the hydraulic conductivity used to create the unsaturated functions. The data for this was collected from Section 3 Column Filtration Testing. Where the average hydraulic conductivity from the first stages of filtration were used for the AMD Slurry and the steps to calculate the hydraulic conductivity for the GT500 fabric was done by taking the Flow Rate from Table 19 and putting it into the Darcy's Law equation (Equation 14). In this equation the Flow Rate equates for $\frac{Q}{A}$, so the only value that was needed is the hydraulic gradient (i). Where Equation 15 lists the equation used to calculate the hydraulic head.

$$k = \frac{Q}{iA} \tag{14}$$

$$i = \frac{\Delta h}{L} \tag{15}$$

Since the values for the slurry were calculated from the Column Filtration Testing, the value for L was taken to be 1 cm and the value for the change in head was taken from the average change in head from the start of the first stage of filtration to the end of that stage when there was no change. The value used to calculate for the change in head in this equation was 20 cm. The hydraulic gradient the value used in the Darcy's Law equation was 20. The hydraulic conductivity for the filter cake for each model decreases as time passes because the filter cake thickens and the pore spaces between material decreases. The equations that was used to solve for the hydraulic conductivity for the AMD Slurry is taken from the Falling Head Test listed in Equation 16.

$$k = \frac{aL}{A\Delta t} \ln\left(\frac{h1}{h2}\right). \tag{16}$$

The values taken from the Column Filtration Testing have the dimensions for hydraulic conductivity (cm/s) which have to be converted to m/hr for the Plaxis models. The hydraulic conductivity values that are used for the model are listed in Table 20.

Table 20: Finite Element Modeling Material Hydraulic Conductivity Values

Material	Hydraulic Conductivity (m/hr)
AMD Slurry	1.05×10^{-1}
Filter Cake Stage 1	5.27×10^{-2}
Filter Cake Stage 2	2.64×10^{-2}
Filter Cake Stage 3	1.32×10^{-2}
GT500 Fabric	2.44

5.3.2 Methodology

The model is just the slurry or sludge inside as the center core and the GT500 fabric outlines it where it acts as the filter for water flowing out of the system. The model is created on a four-stage system where the value that changes is the hydraulic conductivity of the slurry that is the proximity of the GT500 fabric. Based on the filter testing, the fabric develops a filter cake build-up over time due to the particle solids clogging the fabric. The increased density of the filter cake decreases hydraulic conductivity. The area of the filter cake is constant with the hydraulic conductivity changing between the 2nd, 3rd, and 4th stage injections. The model's stages were simulated to be 7 days for the first stage and 21 days for the next three stages. A data point is collected and shown for every 24 hours, to show the model changing over time. The overall duration of the model is 1,680 hours (70 days).

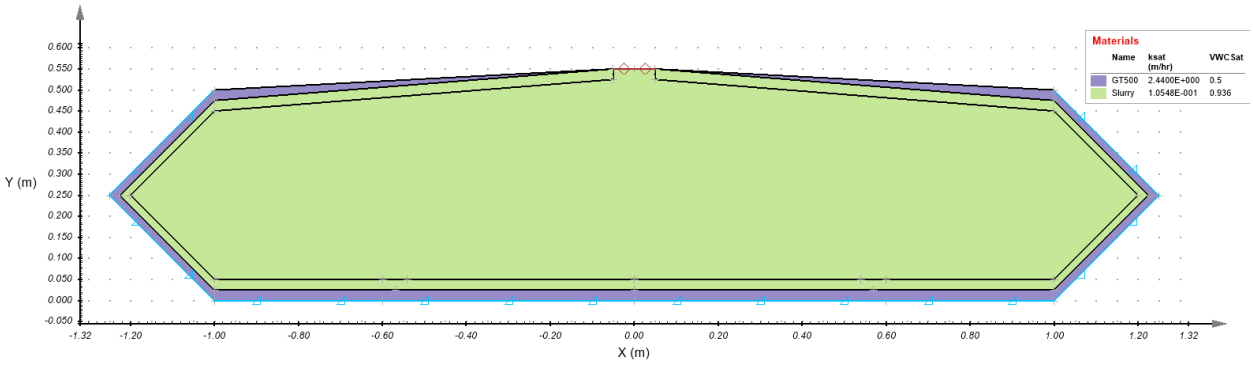

Figure 26: Plaxis Model Design

Figure 26 is the design for the base model in Plaxis. The size of the model was created in a range to simulate the cross section of a geotextile tube that is currently in the field. The dimensions of the model have a length of 2 meters and a heigh of 0.5 meters. The area for the GT500 fabric in the model is not consistent with the thickness that is typically found out in the field. The thickness for the filter cake in the 2nd, 3rd, and 4th stages is the same as the GT500 in the model. In the filter test the thickness decreases over time but maintained a constant area to eliminate another variable to be calculated for.

The AMD slurry injection is at the top center of the model so that the inflow of material is within the geobag volume to simulate the geotextile fabric to only act as radial drainage. Where the darker shaded region is the geotextile, and the lighter shaded region is the AMD slurry. The filter cake region is filled in with the AMD slurry material in the first stage and then changed to the filter cake for the other stages

Both the GT500 fabric and the AMD Slurry was modeled as unsaturated material and required a function that relates hydraulic conductivity to the slurry saturation. The Van Genuchten and Mualem Estimation function was used as listed below.

$$\theta_w = \theta_r + \frac{\theta_s - \theta_r}{(1+(a\varphi)^n)^m} \tag{17}$$

$$k_w = k_s \frac{(1-(a\varphi)^{(n-1)}\{1+(a\varphi)^n\}^{-m})^2}{(1+(a\varphi)^{nm/2}} \tag{18}$$

$$n = \frac{1}{1-m} \tag{19}$$

Where:

k_s is the Saturated Hydraulic Conductivity

k_w is the Hydraulic Conductivity at a particular suction value

θ_w is the Volumetric Water Content

θ_s is the Saturated Water Content

θ_r is the Residual Water Content

φ is the Negative Pore Water Pressure

α, n, and m are the Model Fitting Parameters

The k_s values are taken from Table 19. The values for the AMD slurry saturated water content is calculated using the average water content within a geotextile tube. These values are taken from Section 4 data points. The residual water content in the Van Genuchten function is defined as the water content at a soil suction value of 1500 kPa where this value for soil suction is defined as the wilting point (Vanapali et al., 1998). According to Luckner et al. (1989), the residual water content is specified by the maximum amount of water in a soil that will not contribute to the liquid flow because there is a blockage in the flow paths. The value for the AMD slurry's residual water content is related to the values for a Silt Loam which are taken from the Soil Water Storage Properties from the Minnesota Stormwater Manual which shows the wilting point, residual water content, for different soils. The wilting point value for a loam soil are between 10 to 15% (Northeast Region Certified Crop Advisor, 2010). Based on the research by Bouazza et al. (2006) the saturated water content is typically a large value for non-woven geotextiles with large porosities and the residual water content is small when the suction is high. The value for the GT500 fabric's residual water content are similar to the values from this article while the water content is estimated to be 0.5 to simulate that the bag is the driest at the outside edge.

The model fitting parameters (a, n, and m) for the AMD slurry are also based on values for a Silt Loam (Rawls et al., 1982). In order to calculate the model parameters for the geotextile fabric a computer program called Retention Curve (RETC) (van Genuchten et al., 1991). Bouazza et al. (2006), Stormont & Morris (2000), and Vanapalli et al. (1998) developed values from the RETC program for the geotextile fabrics. The steps that were taken when running the RETC program were to estimate the parameters. The predications are similar to the values for sand since nonwoven geotextiles have similar characteristics to coarse material. The initial estimated values used are shown in Figure 27. RETC uses the sum of squares (SSQ) in order to estimate the values. The SSQ for the estimation of the n parameter is shown in Figure 28.

```
INITial values of the coefficients
==================================
No      Name         INITial value
 1     ThetaR            .0000
 2     ThetaS            .9900
 3     Alpha            5.0000
 4     n                1.0500
 5     m                 .0476
 6     l                 .5000
 7     Ks               2.4400
```

Figure 27: Initially Predicted Parameters from RETC Program (Source: RETC)

```
NIT      SSQ       n
 0    14.43292    1.0500
 1    14.43275    1.2154
 2    14.43235    1.1867
 3    14.43233    1.1790
 4    14.43233    1.1775
 5    14.43233    1.1772
 6    14.43233    1.1772


RSquated for regression of observed vs fitted values =-1.47415934
================================================================


Nonlinear least-squares analysis: final results
===============================================
                                                95% Confidence limits
Variable     Value      S.E.Coeff.     T-Value      Lower        Upper
n           1.17715      2.45320          --       -4.2889      6.6432
```

Figure 28: Sum of Squares from RETC Program (Source: RETC)

The values that were used to create the models based on the Van Genuchten and Mualem Estimation function are listed below in Table 21. With an example of the Plaxis 2D window for inputting the parameters is shown in Figure 29.

Table 21: Van Genucthen and Mualem Estimation Parameters

Material	**a (1/kPa)**	**n**	**Saturated Water Content (θ_s)**	**Residual Water Content (θ_r)**
AMD Slurry	0.048	1.211	0.9361	0.75
GT500	5	1.17715	0.5	0

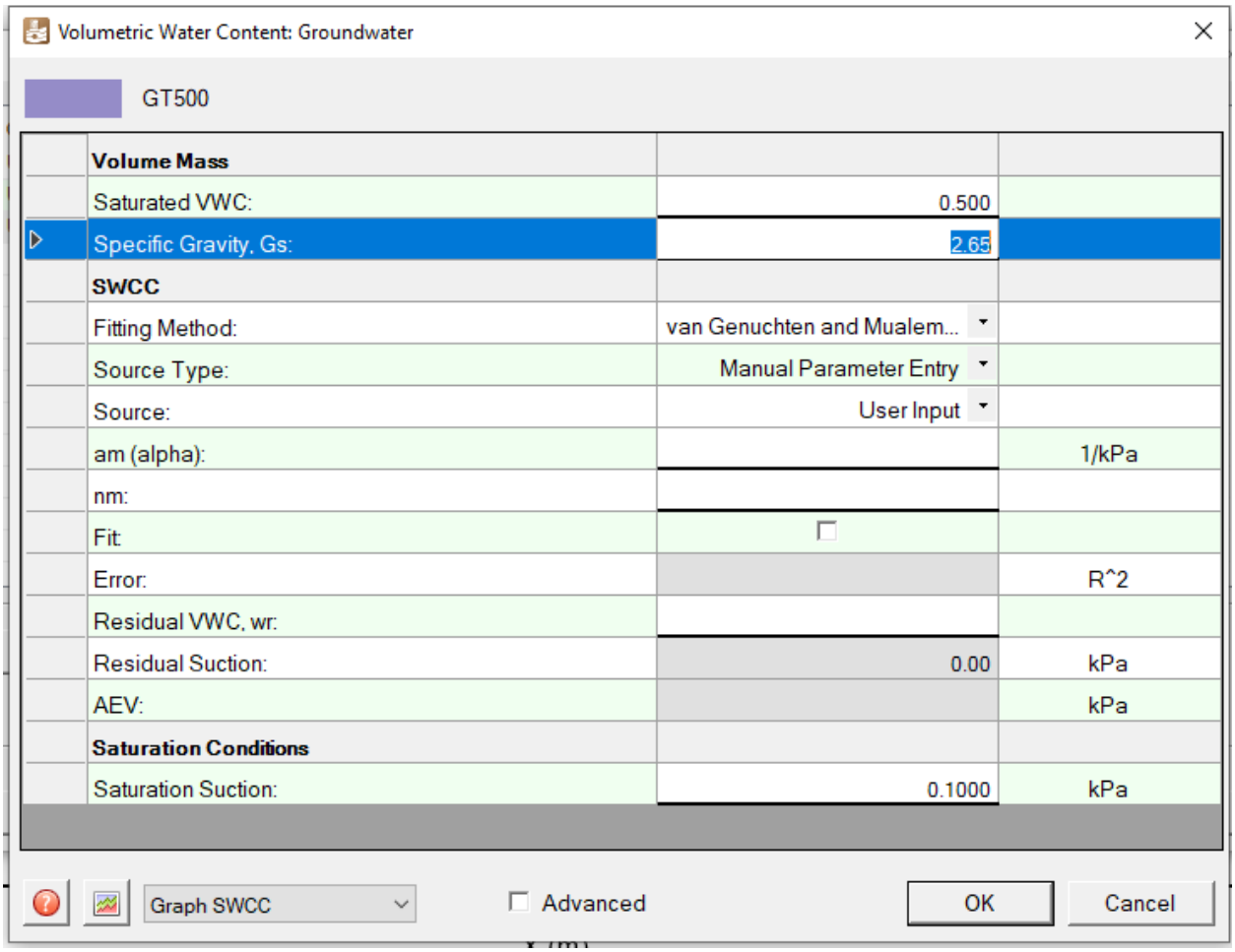

Figure 29: Plaxis 2D Van Genuchten Parameter Input Window (Source: Plaxis 2D)

The models that were developed in Plaxis 2D are listed in Table 22, with a brief description of what each model is showing. In total there are 9 output models and 1 input model (Shown in Figure 26).

Table 22: Plaxis Output Models

Model #	Description
1	Hydraulic Conductivity Under Flow
2	Hydraulic Conductivity with Filter Cake Build Up
3	Initial Water Content
4	Water Content on Final Day of Stage 1
5	Water Content with Addition of Filter Cake
6	Final Water Content
7	Solids Content Distribution
8	Expected Moisture Flow
9	Unexpected Moisture Flow

5.3.3 Boundary Conditions

Boundary conditions (BC) are displacements assigned to the edges of the regions of the Plaxis model. In Figure 26 the Plaxis model has boundary conditions that are placed on the lines the connect the regions and along the edge of the geotextile region. The boundary conditions that are: 1) the infiltration or inflow of water, which are weather conditions; 2) zero flux, meaning no flow through the zone; and 3) a unit gradient, which generates the flux outward of the model to be equal to the hydraulic conductivity. The value for the inflow is $850 m^3/hr/m^2$ is allowed to flow into the model for the first 12 hours of each week (or every 7 days) then continue for the next 156 hours as the water dewaters out of the model. The inflow is only allowed to enter the center port, shown in Figure 30, which shows an inflow of water and how many times water is input into the model's system. Where the AMD slurry injection flow rate is in cubic meters per hour. The zero-flux boundaries are along the top of the model, so the inflow is only allowed to flow through the injection port and not through the geotextile that immediately borders the injection port. The unit gradient boundary conditions are placed to surround the geotextile region, this is so that the injected flow of the material through the slurry region goes into the geotextile based on its hydraulic conductivity and then the material flows through the geotextile and out of the model based on the hydraulic conductivity of the geotextile fabric.

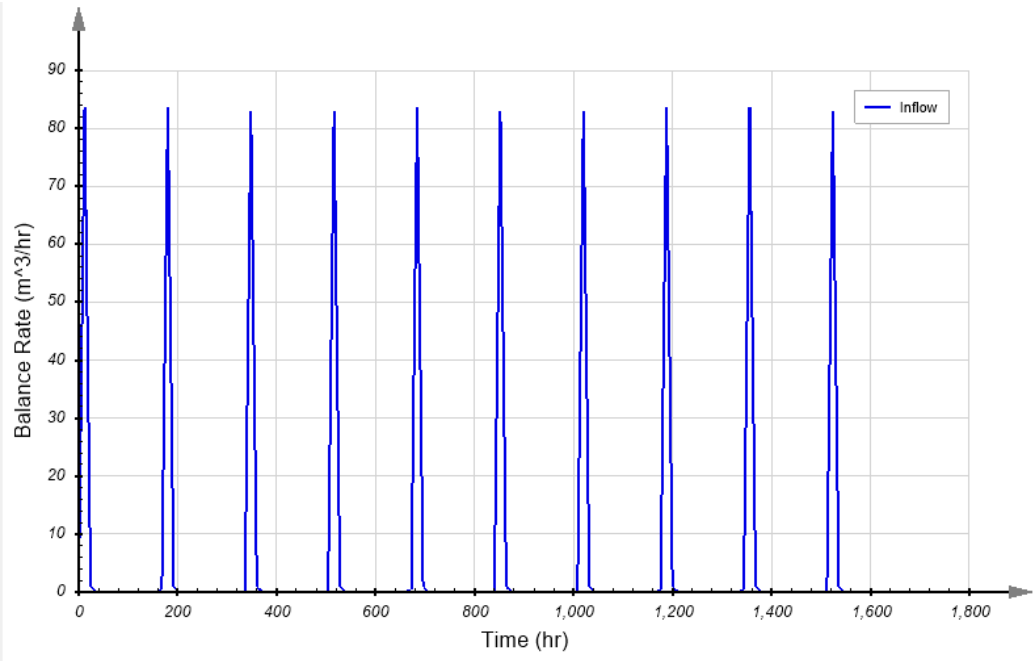

Figure 30: Plaxis Models Inflow Graph (During Injection)

5.4 Results and Inferences from Analysis

5.4.1 Hydraulic Conductivity

The first discussion of results will be based on the hydraulic conductivity changes due to the variation in the density of the filter cake. The Plaxis model resulted in 2 significant output models that show how the hydraulic conductivity changed during the models duration. Model #1 in Figure 31 show as water flows throughout region and has a relatively large contour range due to the low hydraulic conductivity ($2.93x10^{-3}$ cm/s or $1.05x10^{-1}$E m/hr) used for the slurry and the relatively large value for the GT500's permittivity. Model #2 in Figure 32 shows there is limited flow out (dewater) of the system, and the buildup of the filter cake. The built-up filter cake is evident of the steep increase in hydraulic conductivity in the proximity of the geotextile fabric. This region has a consistent hydraulic conductivity throughout the system in the AMD slurry region, and the hydraulic conductivity for the filter cake changes between stages of the model, meaning as the stages progress the flow through that zone decreases.

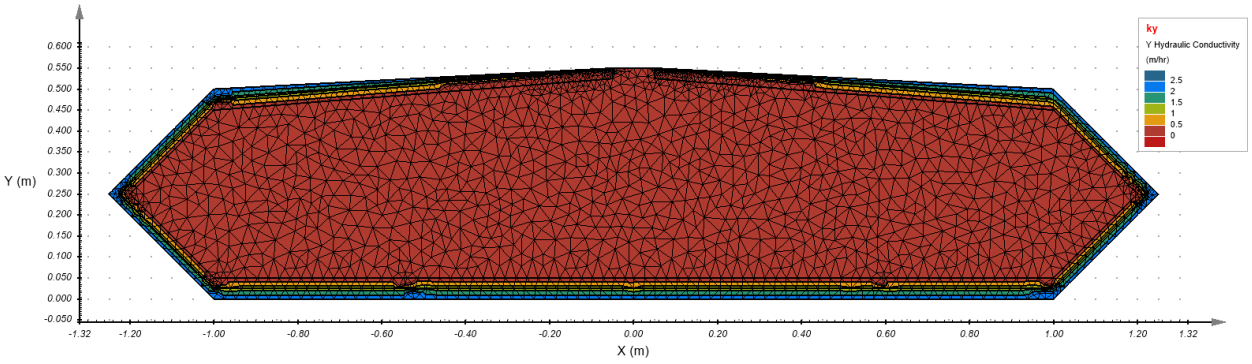

Figure 31: Plaxis Model #1 - Hydraulic Conductivity under Flow

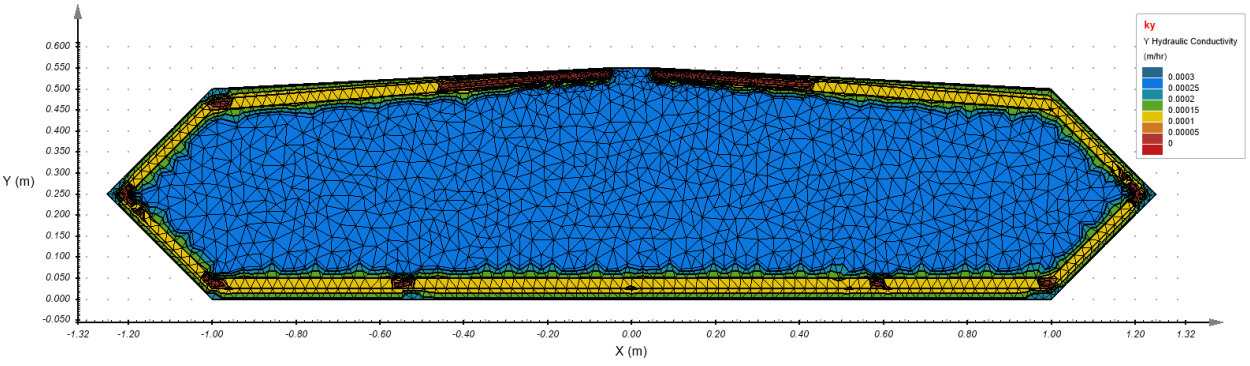

Figure 32: Plaxis Model #2 - Hydraulic Conductivity Filter Cake Build Up

The color scheme for these models has the blue regions being the larger hydraulic conductivity and the red region being the smallest hydraulic conductivity. So, for Figure 31 the outer zone,

where the GT500 fabric is, has permittivity. In Figure 32 the AMD slurry's region has a larger hydraulic conductivity than the material that is in the vicinity of the filter cake and the inner edge of the GT500 fabric.

5.4.2 Water Content

The next discussion of model analysis outputs addresses the changes in water content over time throughout the system. The models that were collected from the water content can be compared with the field sampling in Section 4. These models are to predict water content percent when AMD sludge is pumped into a bag that already has a slurry sludge mixture inside. The models which have the largest relevance when looking at the water content occur from the first stage and the final day of the first stage, then when AMD sludge is pumped into the system and then the final model from the fourth stage. Each model has the same scale for comparison. Model #3 in Figure 33 has only the GT500 fabric and the AMD slurry. In this model the fabric is defined as a clogged zone with a moisture content of 50% and the AMD slurry has its water content set at 93%. Model #4 in Figure 34 is the final day of stage 1 where the internal area's water content is expected to decrease, and the water content decreases as the material gets closer to the GT500 fabric shown by the increase in contour lines.

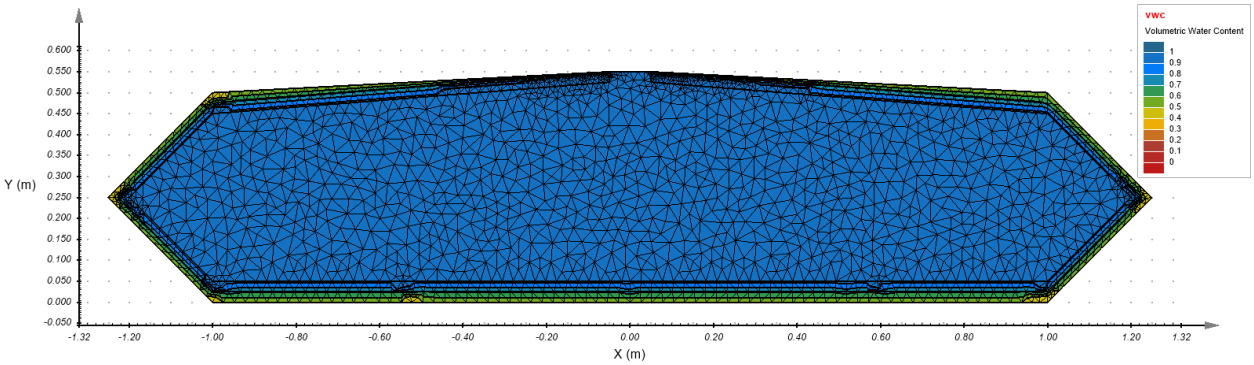

Figure 33: Plaxis Model #3 - Water Content Initial Model Results

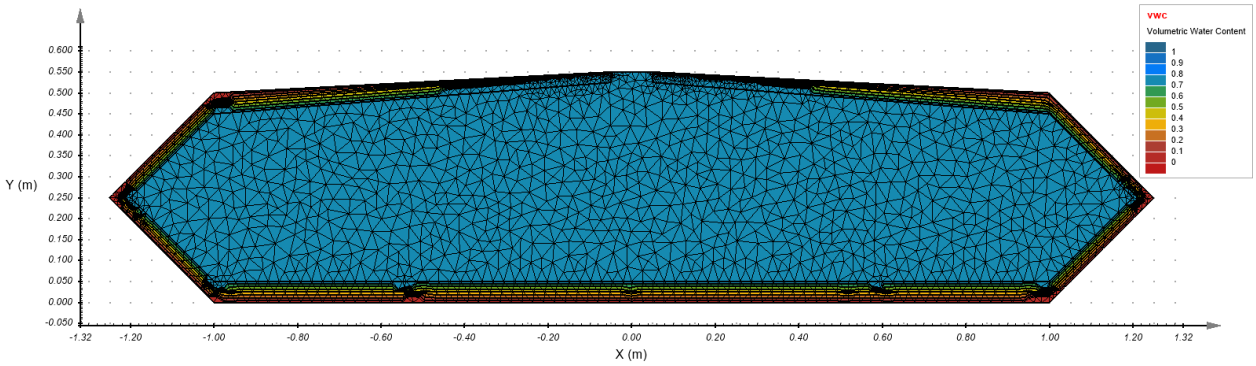

Figure 34: Plaxis Model #4 - Water Content First Stage Final Day Results

The next two output models include the filter cake. Where Model #5 in Figure 35 is showing the output from the first day of stage 2. Model #6 Figure 36 shows that the center regions water content increases back to the initial water content because of the inflow of more AMD slurry. Comparing this figure to the initial results in Figure 33 the main difference is that the filter cakes region has a lower water content, because of the density of the filter cake. Figure 36 from the final output is similar to the final day from the initial stage with the main difference being the region near the top center because of the introduction of the filter cake that there is a change in water content in that region that was originally just AMD slurry in Figure 34.

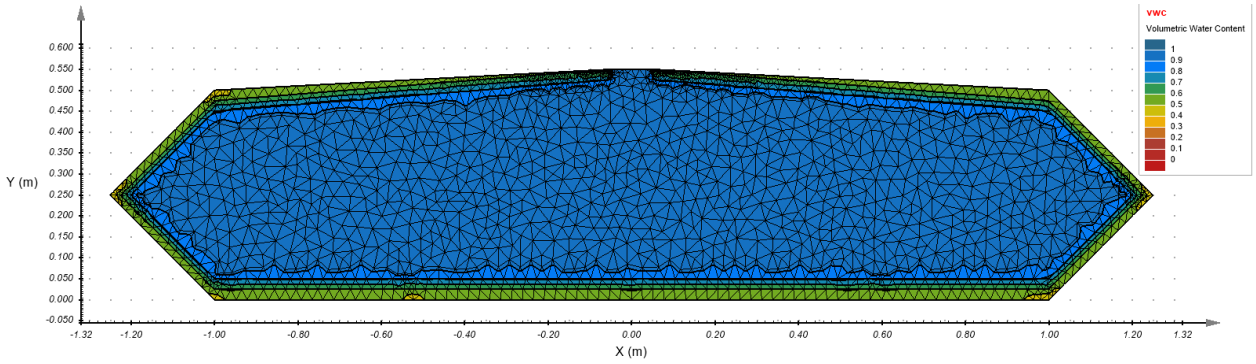

Figure 35: Plaxis Model #5 - Water Content Addition of Filter Cake Results

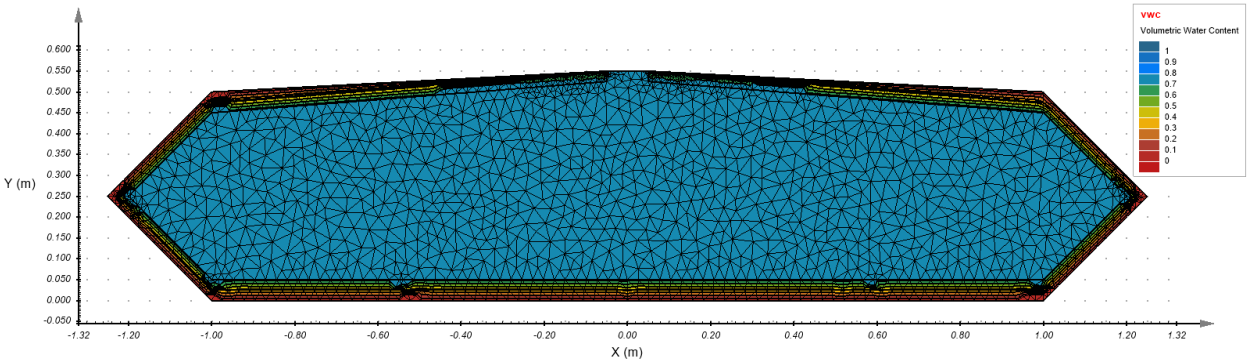

Figure 36: Plaxis Model #6 - Water Content Final Model Results

5.4.3 Total Solids Content

The distribution of total solids content in the AMD Sludge is discussed in this analysis shows the largest solids content region and to maximize for higher solids percentage throughout the geotextile tube cross section. An important finding is that the change in solids content over time and with the addition of AMD slurry is that there was no change. This means there is a difference between the metrics used to calculate the solids content and the water content. This is due to the water content calculation is based on volumetric water content (equation 17). Model #7 in Figure 37 is the model showing the distribution of the solids content within the system. Where the model shows that the solids content within the AMD slurry is about 15% and majority of the solids is within the region for the GT500 fabric, and some contour lines are shown to be within the filter cakes region.

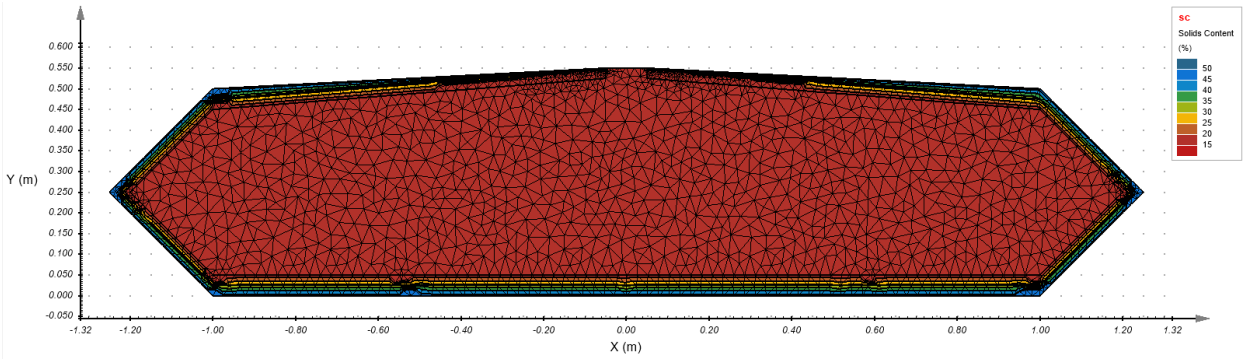

Figure 37: Plaxis Model #7 - Total Solids Content Distribution

5.4.4 Moisture Flow

This analysis addresses how the moisture is expected to dewater within the geotextile tubes. The direction to show this result was by creating stream tracers within the system at different time steps for the model. This illustrates that the flow of moisture is inconsistent between the stages of

the model and where the water is expected to dewater. Model #8 in Figure 38 shows the flow of material during the first stage, but it is also the predicted flow throughout most of the models duration. The figure shows that the flow in the system is symmetrical, and all saturated flow lines are originating from the midpoint of the inflow port.

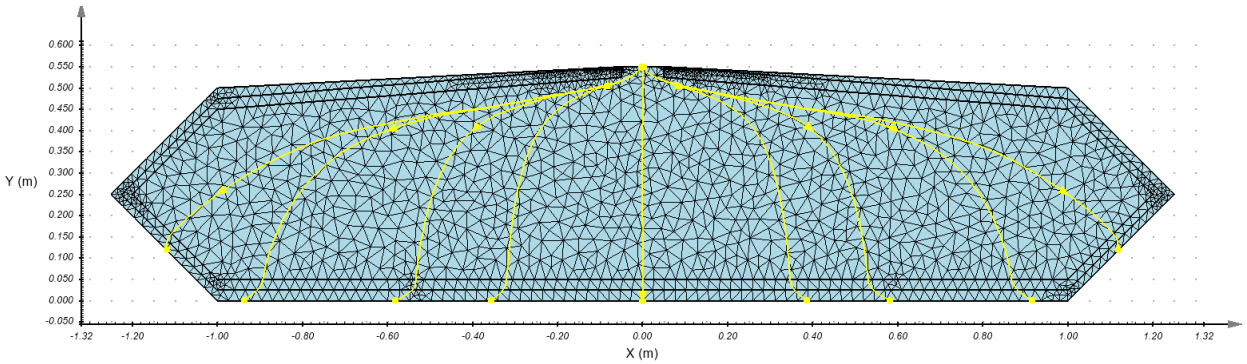

Figure 38: Plaxis Model #8 - Expected Moisture Flow

Model #9 in Figure 39 shows a second model displayed for moisture flow at the end of each week prior to a second pumping into the system. The results illustrate the AMD slurry flows from the filter cake region up to the input port and flows through GT500 region before flowing out of the system at the bottom. This output creates a problem in the Plaxis model because it simulates that the moisture will flow inwards and around the GT500 fabrics outline. The goal of the model is to only allow moisture to flow out of the system once it flows through the GT500 fabric.

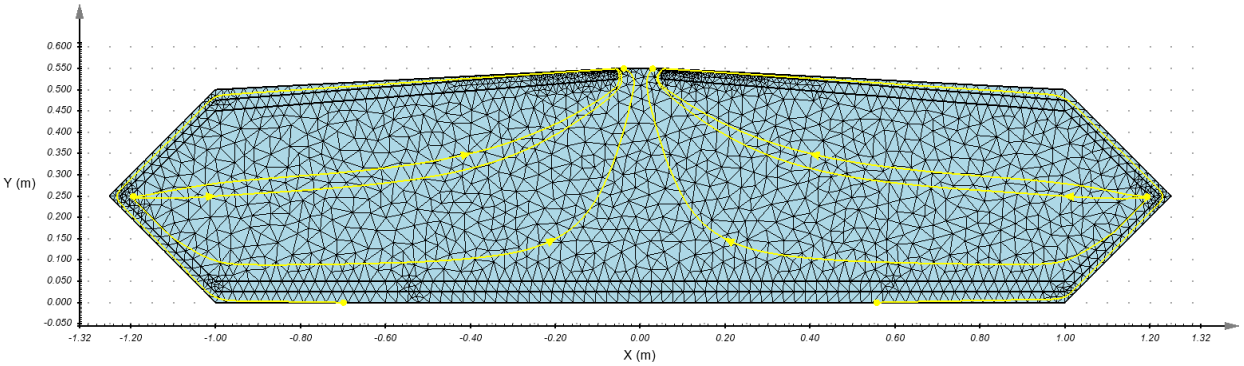

Figure 39: Plaxis Model #8 - Unusal Moisture Flow

5.5 Numerical Model Findings

A finite element model was developed for analysis of moisture flow inside a geotextile tube using Plaxis 2D. The Plaxis 2D Groundwater results were able to predict the change in hydraulic conductivity (filter development) and the change in water content (drainage) in a cross-sectional profile of a geotextile tube calibrated using field and lab data. The models shown here are used to show what the expected flow in a geotextile tube is right now. The lateral drains were not included in modeling due to the inability to make it work in Plaxis 2D. In future work there will be models created in order to show how the introduction of a drainage core in the center would change the flow paths and all the other components.

The significant findings from the modeling are:

1) The expected unsaturated flow has the flowlines traveling radially towards the external geotextile layer. With hydraulic mounding occurring, where the oldest material is displaced to the bottom of the cross section.
2) By showing an increase in filter cake buildup it is expected there to be an increase in solids around the geotextile and there to be a decrease in dewatering out of the system.
3) In comparison to the moisture distribution testing the results from the expected (modeled) moisture content does not equal the values that were collected from the field (no effective calibration).
4) In comparison to the column filtration testing the hydraulic conductivity is expected to reduce and the filter cake thickness is expected to increase.
5) The AMD Total Solids are not predictable in field geobags

6.0 Conclusions

The purpose and objective of this research was to develop and investigate a cost-effective method that will enhance the dewatering of high moisture content sludge in geotextile tubes by non-mechanical means. The research is done to evaluate the use of internal drains and their effectiveness in increasing the dewatering efficiency and increase the total solids percentage inside the geotextile tubes.

6.1 Significant Findings

Significant findings from the research are presented in the sections below.

6.1.1 Column Filtration Testing

1) With and without polymer the 1100N nonwoven fabric has the highest filtration efficiency
2) Without polymer the MD88 Typar fabric has the higher filtration efficiency (95.61% vs 94.7%) but has a lower hydraulic conductivity which means the fabric clogs faster than the MD7407 Typar fabric
3) The amount of polymer affects the hydraulic conductivity. The 20 ppm T&T material's hydraulic conductivity stabilized at 3E-05 cm/s and the Raw (no polymer) Omega material stabilized at 3E-04 cm/s
4) The system's (filter cake + geotextile) hydraulic conductivity was found to be independent of the geotextile used. This implies that the filter cake hydraulic conductivity controls drainage. The drainage process requires that the geotextile filter is developed, and a stable filter cake is developed.
5) The Apparent Opening Size (AOS) of the fabric had an effect on the clogging of the fabric. Where fabrics with a smaller AOS (MD88) clogged faster than those with a larger AOS (GT500). This process impacts whether the fabric blinds-off drainage flow or whether a stable filter cake is formed. For the lateral drainage, the prefabricated vertical drain and typar fabric blinds-off and does not develop a lower hydraulic conductivity filter before the larger AOS geobag fabric does. The typar fabric blinding diminishes drainage (10X) compared to the nonwoven geotextiles (1100N and 140NC).

6.1.2 Moisture Distribution Testing

1) There is no clear trend in the moisture profiles that indicate preferential sludge dewatering
2) There are no preferential drainage paths which indicate there are no clear placement of the lateral drains
3) Moisture within the geotextile tubes have to do with the use of a polymer, the polymer dose, the injection time, and the tube's age.
4) It is not possible to differentiate the zones of high polymer or low polymer within the geotextile tubes

6.1.3 Finite Element Modeling

1) The expected unsaturated flow has the flowlines traveling radially towards the external geotextile layer. With hydraulic mounding occurring, where the oldest material is displaced to the bottom of the cross section.
2) By showing an increase in filter cake buildup it is expected there to be an increase in solids around the geotextile and there to be a decrease in dewatering out of the system.
3) In comparison to the moisture distribution testing the results from the expected (modeled) moisture content does not equal the values that were collected from the field (no effective calibration).
4) In comparison to the column filtration testing the hydraulic conductivity is expected to reduce and the filter cake thickness is expected to increase.
5) The AMD Total Solids are not predictable in field geobags.

6.2 Lateral Drainage Applications

Possible applications for the use of lateral drains in the geotextile bags are:

1) The AMD sludge permeability and first exposure fill appear to be the limiting factor for geotextile efficiency.
2) The use of lateral drains may be effective using the existing typar and nonwoven fabrics
3) Need to continue numerical modeling trials to incorporate lateral drainage function.

6.3 Future Work

Creating a model that correctly depicts all the elements that occur when treating AMD at a treatment plant is extremely complicated. A model that could show the initial filling stage of a geotextile tube with the AMD slurry being pumped in where the total solids and the particle size can be depicted in the inflow equation would be more accurate of a model to show the flow inside a tube and how to expect it to dewater.

The next stage in the modeling process for this research topic is to add a drain core into the center of the cross section and show how the moisture in the AMD sludge is expected to flow. The addition of a drain core will help answer the research question of if an internal drain could help the geotextile tube be more efficient in dewatering and thus could create a more cost-effective geotextile tube design.

References

Akcil, A., & Koldas, S. (2006). Acid mine drainage (AMD): Causes, treatment and case studies. *Journal of Cleaner Production*, *14*(12-13), 1139–1145. https://doi.org/10.1016/j.jclepro.2004.09.006

ASTM D2216-19 Standard test methods for laboratory determination of water (moisture) content of soil and rock by mass. ASTM International - Standards Worldwide. (2019). Retrieved from https://www.astm.org/standards/d2216

ASTM D4491-22 Standard test methods for water permeability of geotextiles by permittivity. ASTM International - Standards Worldwide. (2022). Retrieved from https://www.astm.org/standards/d4491

ASTM D4751-21 Standard test methods for determining apparent opening size of a geotextile. ASTM International - Standards Worldwide. (2021). Retrieved from https://www.astm.org/standards/d4751

ASTM D5088-20 Standard practice for decontamination of field equipment used at waste sites. ASTM International - Standards Worldwide. (2020). Retrieved from https://www.astm.org/d5088-20.html

ASTM D854-14 Standard test methods for specific gravity of soil solids by water pycnometer. ASTM International - Standards Worldwide. (2014). Retrieved from https://www.astm.org/standards/d854

Azevedo, M., & Zornberg, J. (2013). Capillary barrier dissipation by new wicking geotextile. *Advances in Unsaturated Soils*, 559–565. https://doi.org/10.1201/b14393-88

Bentley Systems. (2022). Plaxis CONNECT Edition V20.1. *Bentley*. computer software. Retrieved from https://www.bentley.com/software/plaxis-2d/.

Berilgen, S. A., Tonaroğlu, M., Akgüner, C., & Bulut, B. T. (2016, September). *Dewatering of Dredged Sludge with Geotubes: Effects of Polymer Additive Type and Amount*. Retrieved from https://www.researchgate.net/publication/311593453_Dewatering_of_Dredged_Sludge_with_Geotubes_Effects_of_Polymer_Additive_Type_and_Amount

BishopWater. 2019. How to simplify sludge management for acid mine drainage (AMD) treatment. Available at: https://bishopwater.ca/sludge-management-amd/

Bouazza, A., Zornberg, J. G., McCartney, J. S., & Nahlawi, H. (2006). Significance of Unsaturated Behaviour of Geotextiles in Earthen Structures. *Australian Geomechanics Journal, Vol. 41, No. 3*, pp. 133–142.

Brink, N., Hyeong-Joo, K., & Znidarcic, D. (2015). *Numerical modeling procedures for consolidation of fine-grained* ... Retrieved from https://www.researchgate.net/publication/277572424_NUMERICAL_MODELING_PROCEDURES_FOR_CONSOLIDATION_OF_FINE-GRAINED_MATERIALS_IN_GEOTEXTILE_TUBES

Cantré, S. (2002). Geotextile tubes—analytical design aspects. *Geotextiles and Geomembranes*, *20*(5), 305–319. https://doi.org/10.1016/s0266-1144(02)00029-8

Fowler, J., Bagby, R. M., & Trainer, E. (n.d.). *Dewatering Sewage Sludge with Geotextile Tubes.* Retrieved from https://www.arieng.com/dosyalar/sayfa/sludge.pdf

Gabr, M. A., Quaranta, J. D., Cook, E. E., & Mooney, D. T. (1997, May 25). *Prefabricated vertical drains in geotechnical engineering: State of the art review*. OnePetro. Retrieved February 2, 2023, from https://onepetro.org/ISOPEIOPEC/proceedings/ISOPE97/All-ISOPE97/ISOPE-I-97-110/23802

Gaffney, D. A., Chambers, M., Fatheringham, C., & Munoz, R. (2011). The value of chemical conditioning with geotextile tube dewatering. *Geo-Frontiers 2011*. https://doi.org/10.1061/41165(397)220

Hogg, R. (2000). Flocculation and dewatering. *International Journal of Mineral Processing*, *58*(1-4), 223–236. https://doi.org/10.1016/s0301-7516(99)00023-x

Indraratna, B., Bamunawita, C., Redana, I. W., & McIntosh, G. (2003). Modelling of prefabricated vertical drains in soft clay and evaluation of their effectiveness in practice. *Proceedings of the Institution of Civil Engineers - Ground Improvement*, *7*(3), 127–137. https://doi.org/10.1680/grim.2003.7.3.127

Jana, A., & Dey, A. (2017). Combined functioning of geotextile as barrier and drainage material in unsaturated Earth retaining structures. *Indian Geotechnical Journal*, *48*(2), 342–359. https://doi.org/10.1007/s40098-017-0268-0

JMP Statistical Discovery LLC. (2021, March). JMP Version (16.2). Retrieved from jmp.com.

Kalin, M., Fyson, A., & Wheeler, W. N. (2006). The chemistry of conventional and alternative treatment systems for the neutralization of acid mine drainage. *Science of The Total Environment*, *366*(2-3), 395–408. https://doi.org/10.1016/j.scitotenv.2005.11.015

Koerner, R. M. (1998). Designing with Geotextiles. In *Designing with geosynthetics* (pp. 84–91). essay, Prentice Hall.

Kutay, M. E., & Aydilek, A. H. (2004). Retention performance of geotextile containers confining geomaterials. *Geosynthetics International*, *11*(2), 100–113. https://doi.org/10.1680/gein.2004.11.2.100

Lawson, C. R. (2008). Geotextile containment for hydraulic and Environmental Engineering. *Geosynthetics International*, *15*(6), 384–427. https://doi.org/10.1680/gein.2008.15.6.384

Li, T., Zhu, Z., Wang, D., Yao, C., & Tang, H. (2006). Characterization of floc size, strength and structure under various coagulation mechanisms. *Powder Technology*, *168*(2), 104–110. https://doi.org/10.1016/j.powtec.2006.07.003

Liao, K., & Bhatia, S. K. (n.d.). *Geotextile tube: Filtration performance of woven geotextiles under pressure*. Retrieved from https://www.researchgate.net/publication/255570778_GEOTEXTILE_TUBE_FILTRATION_PERFORMANCE_OF_WOVEN_GEOTEXTILES_UNDER_PRESSURE

Luckner, L., Van Genuchten, M. T., & Nielsen, D. R. (1989). A consistent set of parametric models for the two-phase flow of immiscible fluids in the subsurface. *Water Resources Research*, *25*(10), 2187–2193. https://doi.org/10.1029/wr025i010p02187

Nasiadka, C. J. (2022). *Geotextile design and performance for dewatering of rare earth element sludge produced from acid mine drainage* (thesis). West Virginia University.

Northeast Region Certified crop adviser (NRCCA) study resources. Certified Crop Advisor study resources (Northeast region). (n.d.). Retrieved from https://nrcca.cals.cornell.edu/soil/CA2/CA0212.1-3.php#:~:text=The%20volumetric%20soil%20moisture%20content,to%2055%25%20for%20clay%20soils.

Office of Surface Mining Reclamation and Enforcement (OSM). 2017. Reclaiming abandoned mine lands. Retrieved from https://www.osmre.gov/programs/aml.shtm.

Pickles, C. B., & Zornberg, J. G. (2012). Hydraulic Classification of Unsaturated Nonwoven Geotextiles for use in Capillary Barriers. *Proceeding of GeoAmericas 2012, the Second PanAmerican Geosynthetics Conference*, pp. 408–420.

Rawls, W. J., Gish, T. J., & Brakensiek, D. L. (1991). Estimating soil water retention from soil physical properties and characteristics. *Advances in Soil Science*, 213–234. https://doi.org/10.1007/978-1-4612-3144-8_5

Rixner, J. J., Kraemer, S. R., Smith, A. D., & Aldrich, H. &. (1986, September 1). *Prefabricated vertical drains, vol. I: Engineering guidelines.* Welcome to ROSA P. Retrieved February 2, 2023, from https://rosap.ntl.bts.gov/view/dot/25323

Silva, V. L., Gardoni, M. G., & Pimentel, K. C. (2021). Numerical modelling of geotextile tubes filled with gold mine tailings. *Geosynthetics International*, *28*(6), 574–583. https://doi.org/10.1680/jgein.21.00017

Skousen, J, A Sexstone, P Ziemkiewicz. 2000. Acid mine drainage control and treatment. Reclamation of Drastically Disturbed Lands, 2nd ed. American Society of Agronomy, Madison, WI, 131-168

Skousen, J. G., Ziemkiewicz, P. F., & McDonald, L. M. (2019). Acid mine drainage formation, control and treatment: Approaches and strategies. *The Extractive Industries and Society*, *6*(1), 241–249. https://doi.org/10.1016/j.exis.2018.09.008

Soil Water Storage Properties Soil Water Storage properties. Soil water storage properties - Minnesota Stormwater Manual. (n.d.). Retrieved from https://stormwater.pca.state.mn.us/index.php/Soil_water_storage_properties

Stormont, J. C., & Morris, C. E. (2000). Characterization of unsaturated nonwoven geotextiles. *Advances in Unsaturated Geotechnics*. https://doi.org/10.1061/40510(287)10

Thapa, K. B., Qi, Y., Clayton, S. A., & Hoadley, A. F. A. (2009). Lignite aided dewatering of digested sewage sludge. *Water Research*, *43*(3), 623–634. https://doi.org/10.1016/j.watres.2008.11.005

van Genuchten, M. T. (1980). A closed-form equation for predicting the hydraulic conductivity of unsaturated soils. *Soil Science Society of America Journal*, *44*(5), 892–898. https://doi.org/10.2136/sssaj1980.03615995004400050002x

van Genuchten, M. T., Leij, F. J., & Yates, S. R. (1991, December). *The RETC code for quantifying the hydraulic functions of unsaturated soils*. EPA. Retrieved February 8, 2023, from https://cfpub.epa.gov/si/si_public_record_Report.cfm?dirEntryId=130162

van Genuchten, M. T., Simunek, J., Leij, F. J., & Seina, M. (2009). RETC for Windows Version (6.02). *USDA*. Retrieved from https://www.ars.usda.gov/pacific-west-area/riverside-ca/agricultural-water-efficiency-and-salinity-research-unit/docs/model/retc-model/.

Vanapalli, S. K., Sillers, W. S., & Fredlund, M. D. (1998). *The meaning and relevance of residual state to unsaturated soils*. Retrieved from http://by.genie.uottawa.ca/~vanapall/papers/conference/1998/cgs98_residual.pdf

Vass, C. R., Noble, A., & Ziemkiewicz, P. F. (2019). The occurrence and concentration of rare earth elements in acid mine drainage and treatment by-products: Part 1—initial survey of the northern appalachian coal basin. *Mining, Metallurgy & Exploration*, *36*(5), 903–916. https://doi.org/10.1007/s42461-019-0097-z

United State Environmental Protection Agency (USEPA). 2018. Coal Mining Effluent Guidelines. https://www.epa.gov/eg/coal-mining-effluent-guidelines.

Warren, K. A., Gabr, M. A., & Quaranta, J. D. (2006). Field study to investigate wide technology for TCE extraction. *Journal of Geotechnical and Geoenvironmental Engineering*, *132*(9), 1111–1120. https://doi.org/10.1061/(asce)1090-0241(2006)132:9(1111)

Weggel, J. R., & Dortch, J. (2012). A model for filter cake formation on geotextiles: Experiments. *Geotextiles and Geomembranes*, *31*, 62–68. https://doi.org/10.1016/j.geotexmem.2011.10.003

Wei, H., Gao, B., Ren, J., Li, A., & Yang, H. (2018). Coagulation/flocculation in dewatering of sludge: A Review. *Water Research, 143*, 608–631. https://doi.org/10.1016/j.watres.2018.07.029

Zhang, X., Presler, W., Li, L., Jones, D., & Odgers, B. (2014). Use of wicking fabric to help prevent frost boils in Alaskan pavements. *Journal of Materials in Civil Engineering*, *26*(4), 728–740. https://doi.org/10.1061/(asce)mt.1943-5533.0000828

Zinck, J. 2006. Disposal, reprocessing and reuse options for acidic drainage treatment sludge. Poster paper presented at the 7th International Conference on Acid Rock Drainage (ICARD), March 26-30, 2006, St. Louis MO. R.I. Barnhisel (ed.) Published by the American Society of Mining and Reclamation (ASMR)

Appendix A: Hydraulic Conductivity vs Time Plots

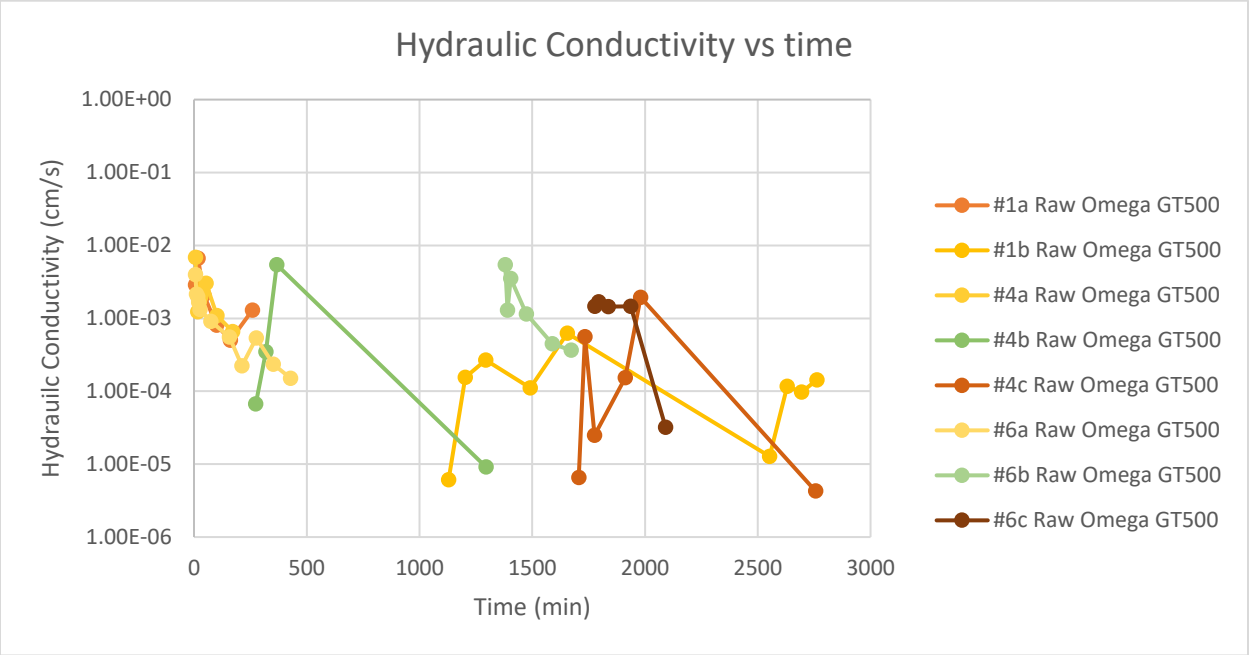

Figure A1: No Polymer Omega Test Set 1 Using GT500 - Hydraulic Conductivity vs Time

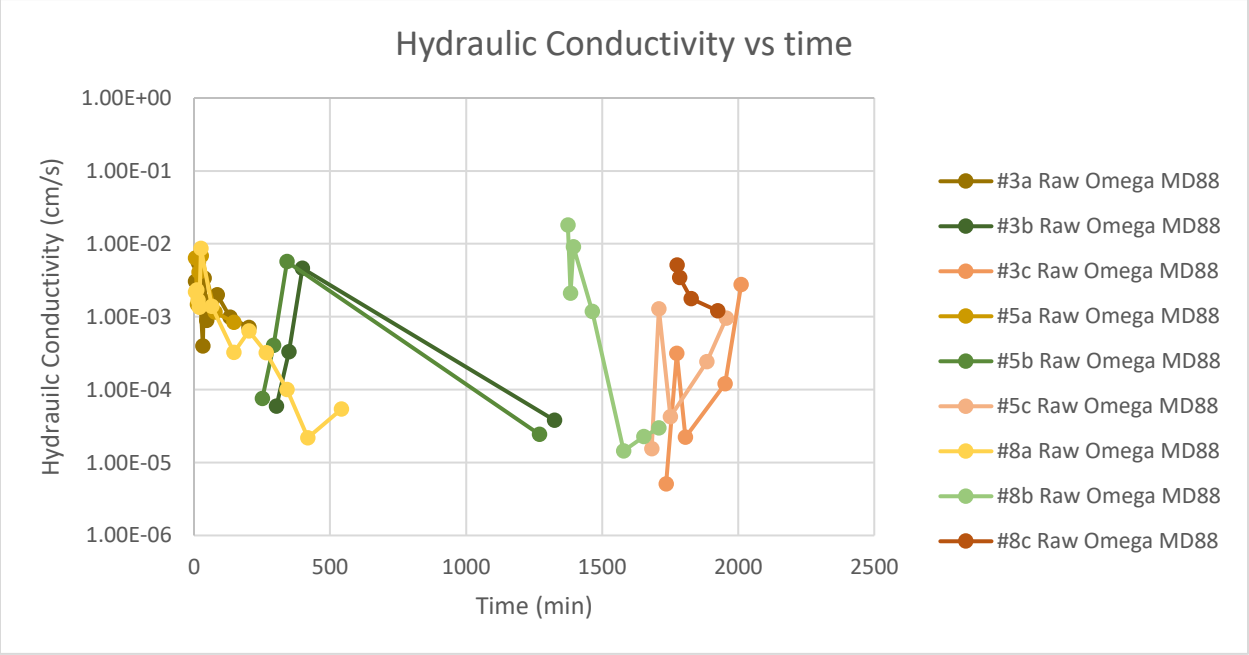

Figure A2: No Polymer Omega Test Set 1 Using MD88 Typar - Hydraulic Conductivity vs Time

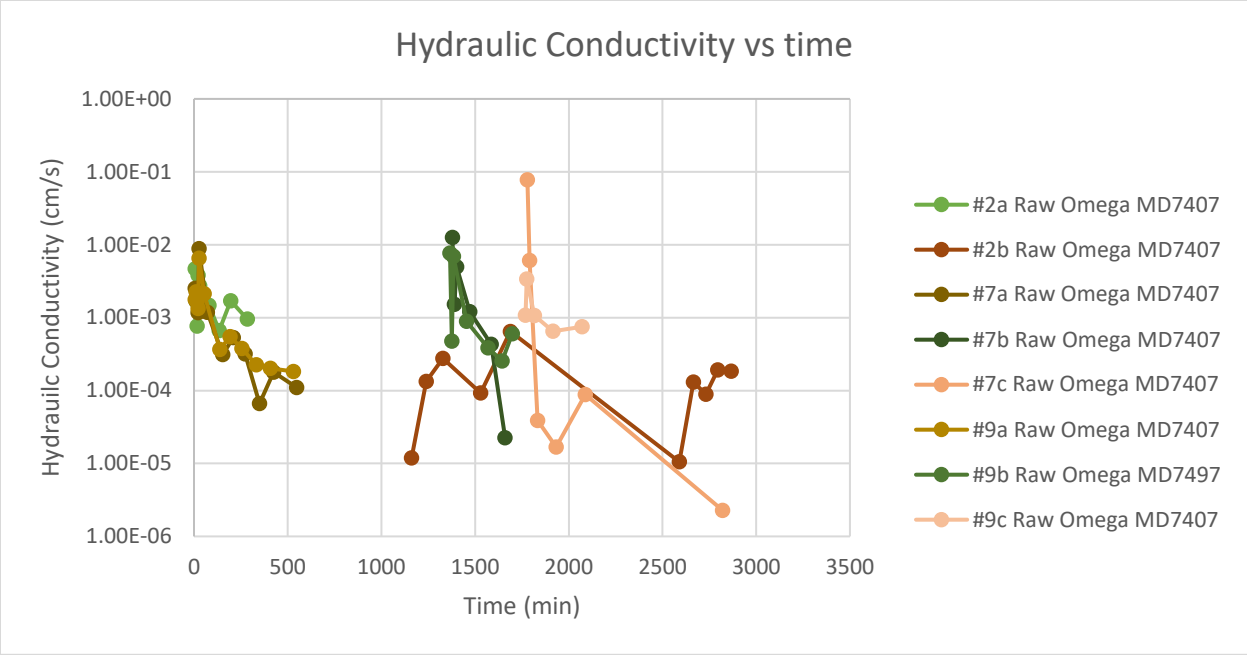

Figure A3: No Polymer Omega Test Set 1 Using MD7407 Typar – Hydraulic Conductivity vs Time

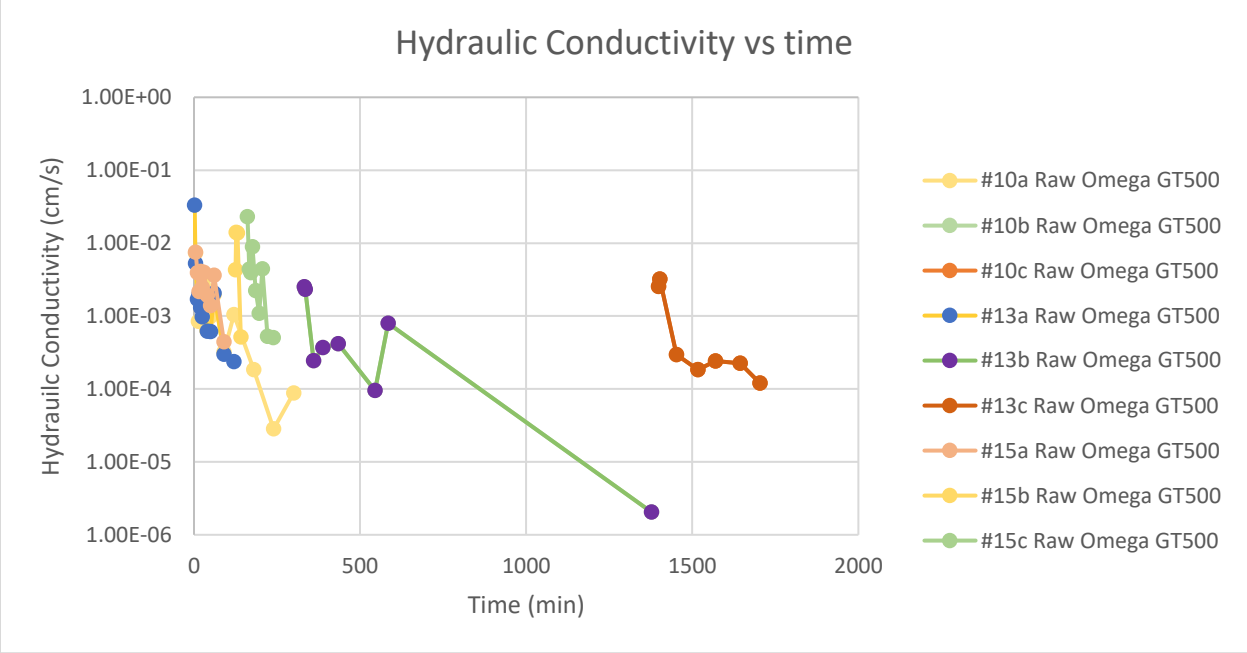

Figure A4: No Polymer Omega Test Set 2 Using GT500 – Hydraulic Conductivity vs Time

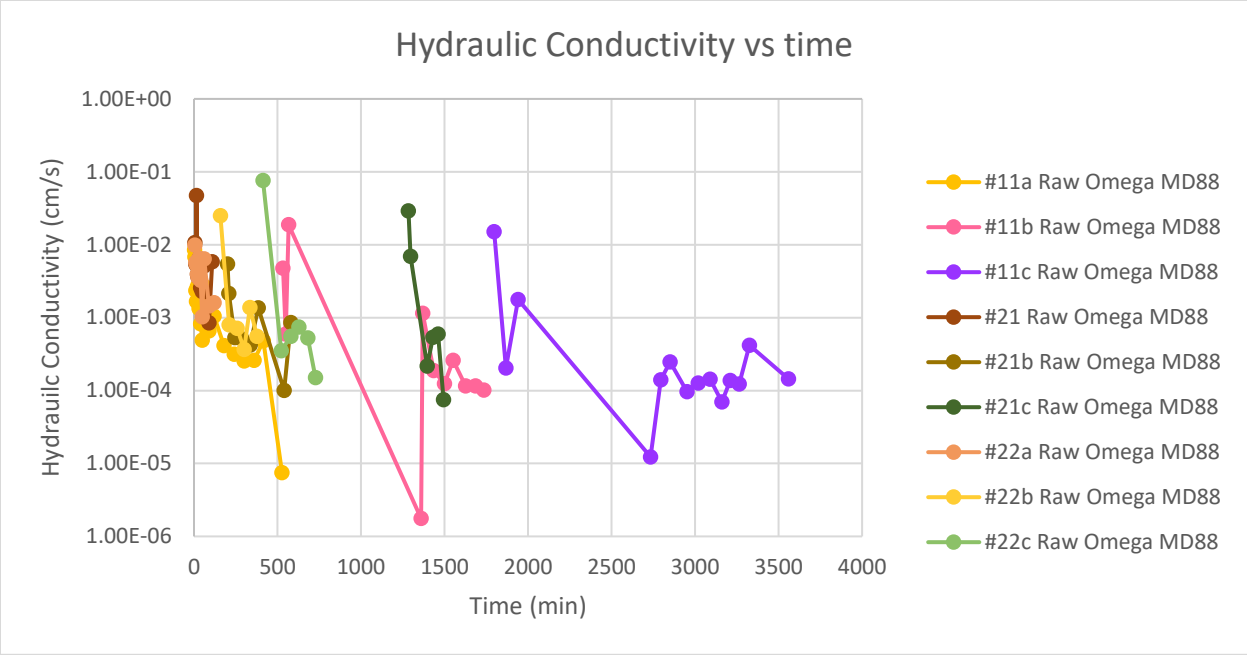

Figure A5: No Polymer Omega Test Set 2 Using MD88 Typar – Hydraulic Conductivity vs Time

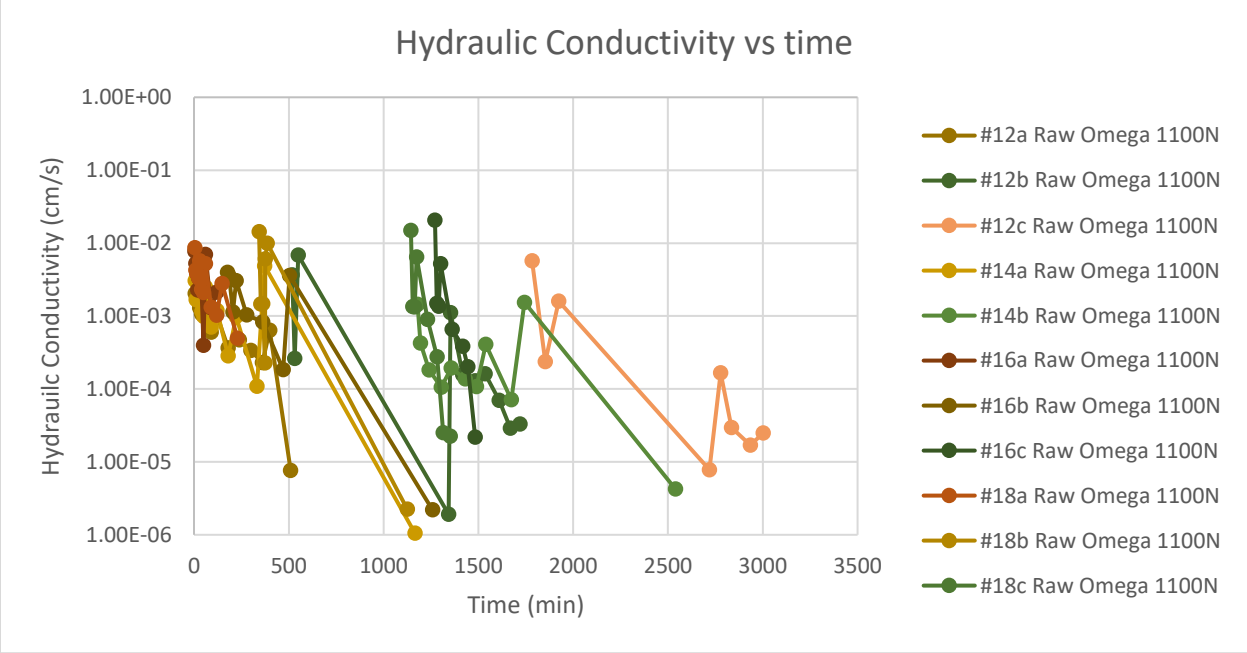

Figure A6: No Polymer Omega Test Set 2 Using 1100N – Hydraulic Conductivity vs Time

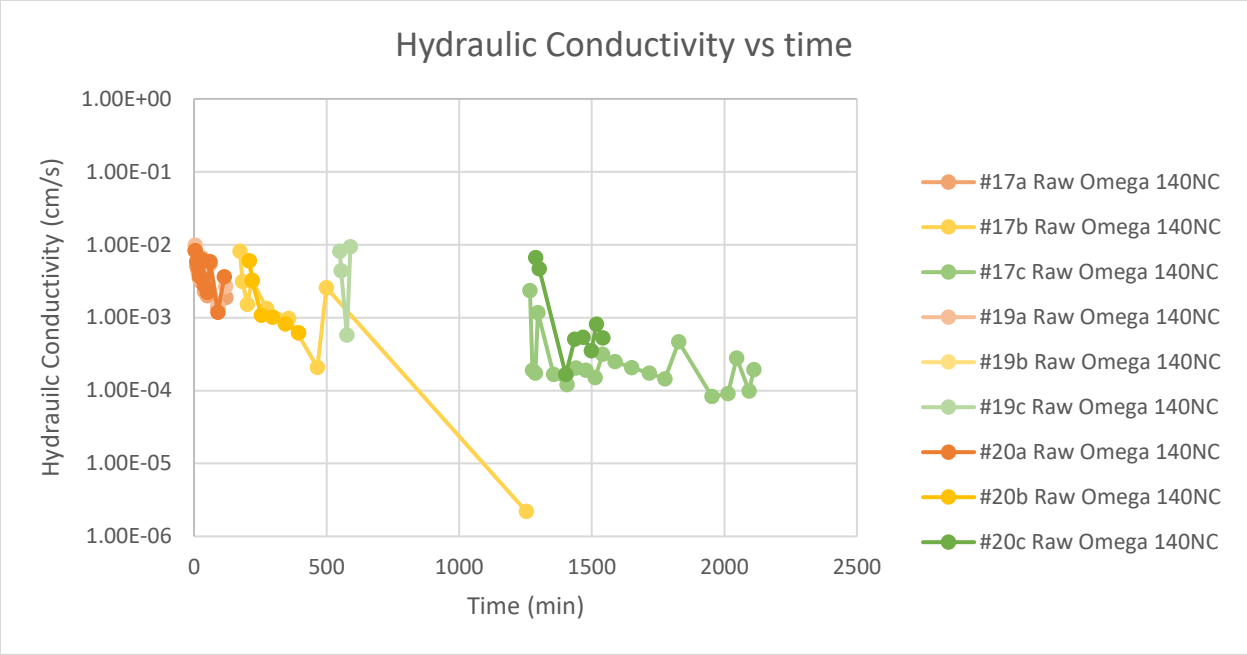

Figure A7: No Polymer Omega Test Set 2 Using 140NC – Hydraulic Conductivity vs Time

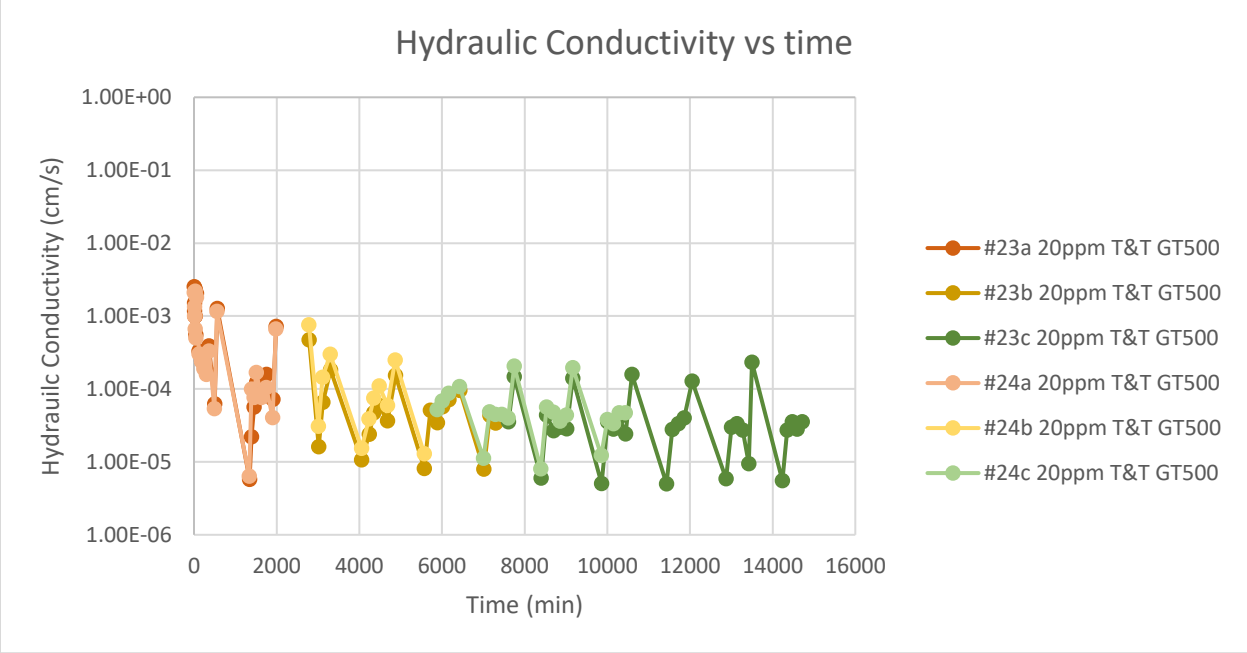

Figure A8: 20 ppm Dosed T&T Using GT500 – Hydraulic Conductivity vs Time

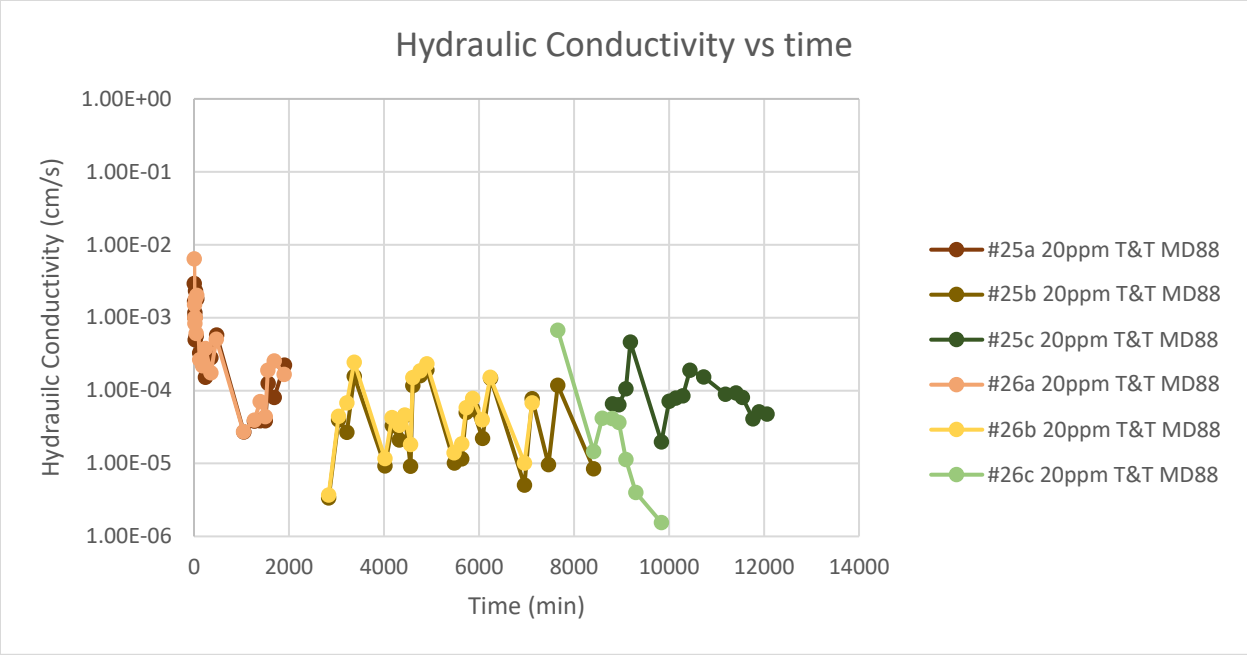

Figure A9: 20 ppm Dosed T&T Using MD88 Typar – Hydraulic Conductivity vs Time

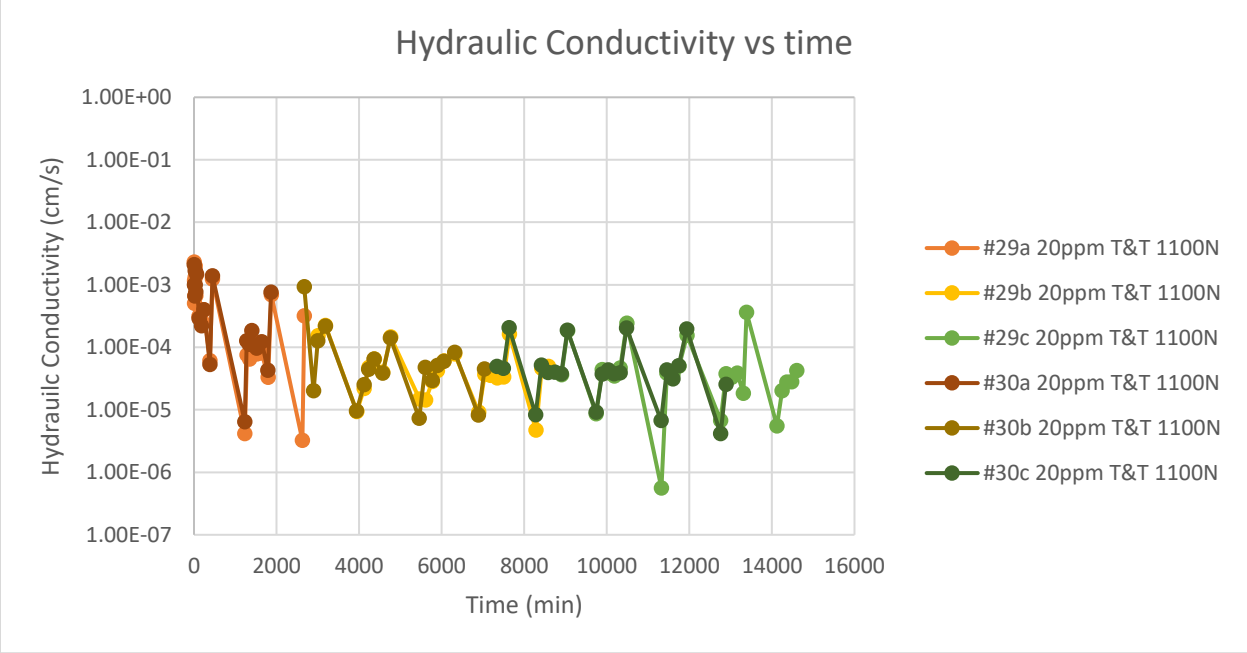

Figure A10: 20 ppm Dosed T&T Using 1100N – Hydraulic Conductivity vs Time

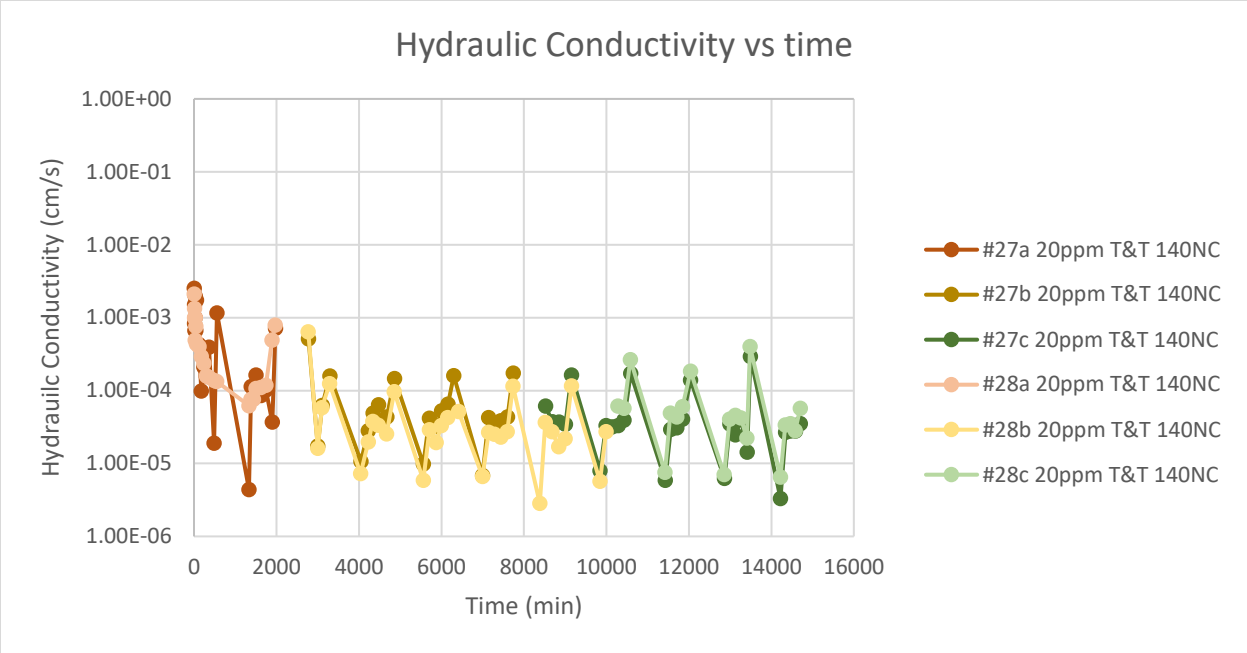

Figure A11: 20 ppm Dosed T&T Using 140NC – Hydraulic Conductivity vs Time

Appendix B: Moisture Distribution Tables

Table B1: Omega Geobag 5 Center Port

5/23/2022	WVU	Jonah Tyson
Bag 5	Cross Section A	Center Port
Depth (cm)	Moisture Content	Total Solids %
0	93.37%	6.63%
10		
20	93.93%	6.07%
30		
40	93.72%	6.28%
50		
60	93.81%	6.19%
70		
80	94.40%	5.60%
90		
100	94.45%	5.55%
110		

Table B2: Omega Geobag 7 Center Port

6/3/2022	WVU	Jonah Tyson
Bag 7	Cross Section A	Center Port
Depth (cm)	Moisture Content	Total Solids %
0	93.67%	6.33%
9		
20	93.62%	6.38%
29		
40	94.75%	5.25%
49		
60	90.78%	9.22%
69		
80	92.64%	7.36%
89		

Table B3: Omega Geobag 7 1.12m Right of Center

6/8/2022	WVU	Jonah Tyson
Bag 7	Cross Section A	1.12m From Center
Depth (cm)	Moisture Content	Total Solids %
0	93.75%	6.25%
9		
20	93.88%	6.12%
29		
40	92.60%	7.40%
49		
60	94.68%	5.32%
69		
80	90.22%	9.78%
89		
100	90.64%	9.36%
109		

Table B4: Omega Geobag 7 2.24m Right of Center

6/8/2022	WVU	Jonah Tyson
Bag 7	Cross Section A	2.24m From Center
Depth (cm)	Moisture Content	Total Solids %
0	93.78%	6.22%
9		
20	88.65%	11.35%
29		
40	94.49%	5.51%
49		
60	93.26%	6.74%
69		
80	92.74%	7.26%
89		
100	93.65%	6.35%
109		

Table B5: Omega Geobag 7 3.05m Right of Center

6/8/2022	WVU	Jonah Tyson
Bag 7	**Cross Section A**	**3.05m From Center**
Depth (cm)	**Moisture Content**	**Total Solids %**
0	93.40%	6.60%
9		
20	93.18%	6.82%
29		
40	92.48%	7.52%
49		
60	94.07%	5.93%
69		
80	94.33%	5.67%
89		

Table B6: Omega Geobag 9 Center Port

9/9/2022	WVU	Jonah Tyson
Bag 9	**Cross Section A**	**Center Port**
Depth (cm)	**Moisture Content**	**Total Solids %**
0	92.55%	7.45%
9		
20	91.29%	8.71%
29		
40	91.54%	8.46%
49		
60	90.69%	9.31%
69		
80	90.19%	9.81%
89		
100	91.52%	8.48%
109		

Table B7: Omega Geobag 1.2m Right of Center

9/9/2022	WVU	Jonah Tyson
Bag 9	**Cross Section A**	**1.2m From Center**
Depth (cm)	**Moisture Content**	**Total Solids %**
0	92.33%	7.67%
9		
20	92.90%	7.10%
29		
40	91.61%	8.39%
49		
60	90.94%	9.06%
69		
80	91.81%	8.19%
89		
100	93.54%	6.46%
109		

Table B8: Omega Geobag 9 2.2m Right of Center

9/9/2022	WVU	Jonah Tyson
Bag 9	**Cross Section A**	**2.2m From Center**
Depth (cm)	**Moisture Content**	**Total Solids %**
0	92.22%	7.78%
9		
20	93.38%	6.62%
29		
40	92.06%	7.94%
49		
60	91.57%	8.43%
69		
80	92.70%	7.30%
89		
100	94.38%	5.62%
109		
120	94.48%	5.52%
129		

Table B9: Omega Geobag 9 3.1m Right of Center

9/9/2022	WVU	Jonah Tyson
Bag 9	Cross Section A	3.1m From Center
Depth (cm)	Moisture Content	Total Solids %
0	89.69%	10.31%
9		
20	90.62%	9.38%
29		
40	90.71%	9.29%
49		
60	92.29%	7.71%
69		
80	94.42%	5.58%
89		
100	93.39%	6.61%
109		

Table B10: Omega Geobag 11 CS A Center Port

11/2/2022	WVU	Jonah Tyson
Bag 11	Cross Section A	Center Port
Depth (cm)	Moisture Content	Total Solids %
0	95.47%	4.53%
9		
20	95.10%	4.90%
29		
40	94.93%	5.07%
49		
60	94.93%	5.07%
69		
80	94.65%	5.35%
89		
100	93.25%	6.75%
109		

Table B11: Omega Geobag 11 CS A 1m Right of Center

11/2/2022	WVU	Jonah Tyson
Bag 11	Cross Section A	1m From Center
Depth (cm)	Moisture Content	Total Solids %
0	95.09%	4.91%
9		
20	94.62%	5.38%
29		
40	94.98%	5.02%
49		
60	94.78%	5.22%
69		
80	94.76%	5.24%
89		
100	93.36%	6.64%
109		

Table B12: Omega Geobag 11 CS A 2m Right of Center

11/2/2022	WVU	Jonah Tyson
Bag 11	Cross Section A	2m From Center
Depth (cm)	Moisture Content	Total Solids %
0	93.57%	6.43%
9		
20	94.00%	6.00%
29		
40	94.65%	5.35%
49		
60	94.53%	5.47%
69		
80	94.83%	5.17%
89		
100	93.02%	6.98%
109		

Table B13: Omega Geobag 11 CS A 2.9m Right of Center

11/2/2022	WVU	Jonah Tyson
Bag 11	Cross Section A	2.9m From Center
Depth (cm)	Moisture Content	Total Solids %
0	93.64%	6.36%
9		
20	94.75%	5.25%
29		
40	94.11%	5.89%
49		
60	94.14%	5.86%
69		
80	92.79%	7.21%
89		

Table B14: Omega Geobag 11 CS B Center Port

11/2/2022	WVU	Jonah Tyson
Bag 11	Cross Section B	Center Port
Depth (cm)	Moisture Content	Total Solids %
0	95.74%	4.26%
9		
20	95.28%	4.72%
29		
40	94.54%	5.46%
49		
60	95.04%	4.96%
69		
80	94.77%	5.23%
89		
100	94.16%	5.84%
109		

Table B15: Omega Geobag CS B 0.8m Right of Center

11/2/2022	WVU	Jonah Tyson
Bag 11	**Cross Section B**	**0.8m From Center**
Depth (cm)	**Moisture Content**	**Total Solids %**
0	95.05%	4.95%
9		
20	95.00%	5.00%
29		
40	95.13%	4.87%
49		
60	95.09%	4.91%
69		
80	94.58%	5.42%
89		
100	94.44%	5.56%
109		

Table B16: Omega Geobag CS B 1.6m Right of Center

11/2/2022	WVU	Jonah Tyson
Bag 11	**Cross Section B**	**1.6m From Center**
Depth (cm)	**Moisture Content**	**Total Solids %**
0	94.90%	5.10%
9		
20	94.87%	5.13%
29		
40	94.60%	5.40%
49		
60	94.85%	5.15%
69		
80	94.10%	5.90%
89		
100	93.78%	6.22%
109		

Table B17: Omega Geobag 11 CS B 2.3m Right of Center

11/2/2022	WVU	Jonah Tyson
Bag 11	Cross Section B	2.3m From Center
Depth (cm)	Moisture Content	Total Solids %
0	93.86%	6.14%
9		
20	94.59%	5.41%
29		
40	94.37%	5.63%
49		
60	94.60%	5.40%
69		
80	93.69%	6.31%
89		

Table B18: Omega Geobag 6 Center Port

1/17/2023	WVU	Jonah Tyson
Bag 6	Cross Section A	Center Port
Depth (cm)	Moisture Content	Total Solids %
0	92.65%	7.35%
9		
20	94.61%	5.39%
29		
40	93.40%	6.60%
49		
60	93.64%	6.36%
69		
80	92.99%	7.01%
89		
100	93.05%	6.95%
109		

Table B19: Omega Geobag 6 0.75m Right of Center

1/17/2023	WVU	Jonah Tyson
Bag 6	Cross Section A	0.75m From Center
Depth (cm)	Moisture Content	Total Solids %
0	93.03%	6.97%
9		
20	94.62%	5.38%
29		
40	93.01%	6.99%
49		
60	93.26%	6.74%
69		
80	93.15%	6.85%
89		
100	93.66%	6.34%
109		

Table B20: Omega Geobag 6 1.5m Right of Center

1/17/2023	WVU	Jonah Tyson
Bag 6	Cross Section A	1.5m From Center
Depth (cm)	Moisture Content	Total Solids %
0	93.11%	6.89%
9		
20	95.10%	4.90%
29		
40	93.49%	6.51%
49		
60	92.77%	7.23%
69		
80	93.78%	6.22%
89		
100	93.54%	6.46%
109		

Table A21: Omega Geobag 6 2m Right of Center

1/17/2023	WVU	Jonah Tyson
Bag 6	Cross Section A	2m From Center
Depth (cm)	Moisture Content	Total Solids %
0	92.75%	7.25%
9		
20	94.75%	5.25%
29		
40	92.80%	7.20%
49		
60	93.02%	6.98%
69		
80	93.59%	6.41%
89		
100	93.58%	6.42%
109		